U.PORTO
FEUP FACULDADE DE ENGENHARIA
UNIVERSIDADE DO PORTO

Master in Chemical Engineering

Department of Chemical Engineering

Application of Simultaneous Thermal Analysis and Mass Spectroscopy on the characterization of Lithium-Sulfur batteries

Master´s Thesis

by

Micael Ângelo Preciso Morais

Developed in the course unit of Dissertation

performed in

DLR – Institute of Technical Thermodynamics

Deutsches Zentrum
für Luft- und Raumfahrt e.V.
in der Helmholtz-Gemeinschaft

Supervisor at FEUP: **Prof. Adélio Mendes**

Supervisor at DLR: **Natalia Cañas**

July, 2013

Acknowledgments

There many people that I have to thank for their contribution to the growth of this work. The first of them is my supervisor at DLR, Natalia Cañas. Since the first day I am really thankful for the huge support given for my integration in a new city, for all the knowledge transmitted, all the time spent and availability to help me with my doubts and for the excellent environment created during the work.

To the leader of the batteries group, Norbert Wagner, for accepted me to work in DLR and for his soccer invitations. To the other members of the batteries group for the collaboration and pleasant atmosphere established, especially to Werner Seybold for his sympathy and enthusiasm during the work.

To my supervisor at FEUP, Professor Adélio Mendes, for supervise my work and for establishing contact with DLR making possible this internship.

To my family, particularly my parents and sister for all the emotional and financial help given during all these months.

To all my friends in Portugal that frequently provided me their support, especially my girlfriend, Inês Almeida and my great friend Luísa Gonçalves for their visits, concern and company given by internet. And also to my friend Ana Baltazar for her previous work at DLR which was a huge help during my research.

To my new friends in Germany for all the good moments shared and assistance given not only during the work but also during the adventures in this city/country.

To SASUP (Serviço de Ação social da Universidade do Porto) for giving the financial support.
At last I would like to show my gratitude to Professor Luís Madeira, for his availability and good collaboration established between DLR and FEUP.

Abstract

Currently, lithium-sulfur batteries (Li-S) are one of the most promising solutions to solve the problems related with energy storage. These batteries present high theoretical specific capacity, high energy density and low cost. Moreover, they are environmental friendly and sulfur is widely abundant. However, some challenges related with the high degradation and fabrication of the batteries components need to be overcome.

This work focuses its investigation in the following topics: cycling stability of Li-S battery using different electrolytes and different C-rate, spectroscopic characterization of the batteries components using several techniques and application of intermediate layer to improve the battery performance.

In the first topic, $LiNO_3$ was tested as additive in the electrolyte. These results were compared with the ones of the other electrolyte without additive. The addition of the additive clearly improved the discharge capacity of the battery increasing its values around 200 Ah/kg during 100 cycles. The coulombic efficiency was also improved obtaining stable values very close to 100%. Microscopic pictures showed the decrease of the quantity of sulfur on the cathodes surface for higher number of cycles and the opposite occurred on the separator surface (anode side). Then it is possible to say that a large part of the sulfur material that leaves the cathode can be found on the other side of the separator. The C-rate analysis showed the best results for 1C-rate. Using a high C-rate the discharge capacity is constant but low, presenting values around 500 Ah/kg. The lowest C-rate studied (0.1) started with high discharge values, however it suffered the highest degradation.

The second topic proved that TGA, DSC and MS are very useful techniques to characterize cathodes before cycling which is a fundamental step to obtain an exact capacity calculation. Three sharp mass loss peaks can be seen in the TGA curves corresponding to weight loss of sulfur, PVDF and CB. Nevertheless, a precise quantification of cathodes after cycling was not possible using TGA.

The microscopic pictures of the separators from the batteries with intermediate layers showed sulfur agglomeration on the separator that means that the nano-porous and micro-porous layers used in this work have not avoided the passage of sulfur to the anode side. These results indicate that no improvement in the discharge capacity at high cycle numbers was achieved.

Key words: Lithium-sulfur battery, simultaneous thermal analysis, mass spectroscopy, intermediate layers, additive for electrolyte

Declaração

Declaro, sob compromisso de honra, que este trabalho é original e que todas as contribuições não originais foram devidamente referenciadas com identificação da fonte.

Contents

List of figures

List of tables

Glossary

List of variables

V	Potential: voltage
$A \cdot s \cdot kg^{-1}$	Specific electrical energy capacity (in this work kg refers to the mass of sulfur)
$J \cdot kg^{-1}$	Specific energy (in this work kg refers to the mass of sulfur)
$mol \cdot dm^{-3}$	Molar concentration
$J \cdot g^{-1}$	Specific enthalpy

List of chemicals

PVDF	Polyvinylidenfluorid
CB	Carbon black
DMSO	Dimethyl sulfoxide
$LiPF_6$	Lithium hexafluorophosphate
$LiNO_3$	Lithium nitrate
TGDME	Tetraethylene glyclol dimethyl ether

List of abbreviations

BSE	Back scatter electron
CDL	Carbon diffusion layer
DSC	Differential scanning calorimetry
EDX	Energy dispersive x-ray
EGA	Evolved gas analysis
EM	Electron microscopy
MS	Mass spectroscopy
PS	Polysulfides
SEM	Scanning electron microscopy
STA	Simultaneous thermal analysis
TGA	Thermo gravimetric analysis
XRD	X-ray diffraction

1. Introduction

1.1 German Aerospace Center (DLR)

DLR (Deutsches Zentrum für Luft- und Raumfahrt e.V. in der Helmholtz-Gemeinschaft) is a German national research center for aeronautics and space, also with extensive research and development in the areas of transportation and energy. All four areas (aeronautics, space, transportation and energy) are integrated into national and international cooperative projects. DLR has approximately 7400 employees at 16 locations in Germany. It has 29 institutes and facilities, spread over 13 sites, as well as offices in Brussels, Paris and Washington D.C. It works in large scale facilities and it promotes the next generation of researchers.

1.1.1 Institute of Technical Thermodynamics (DLR)

This project was developed in the Institute of Technical Thermodynamics in Stuttgart. This institute lies on the field of researching of efficient energy storage systems that conserve natural resources, providing and sustainably development of the countries. It comprises a staff of around 150 scientific and technical employees, engineers and doctoral candidates. The Institute of Technical Thermodynamics also works on selected subjects from the fields of 'Aviation' and 'Transportation', thus contributing to other focal points of DLR. These include developments to the use of fuel cells in aircraft and ground vehicles and to the generation and storage of hydrogen. The Institute and its activities are very well integrated in national and international research networks. Due to the fields in which it researches, the institute acts as a bridge between basic research and industrial development, and thus often plays a key role in the introduction of new technologies.

The "Battery Technology" group, integrated on the DLR Institute of Technical Thermodynamics, focuses its research on the development of new generation of Li-Batteries: Li-Sulfur and Li-Air Batteries due to their theoretical high capacity and energy densities. However these batteries still present many challenges that need to be overcome in order to improve their results. Therefore, this group works with the objective of obtaining reliable batteries using safe materials. The following points are some of its research activities:

- Investigation of degradation processes on the new generation of batteries;
- Determination of status of battery with in-situ diagnostics and frequency analysis;
- Multi-scale-modeling and simulation of electrochemical processes in the batteries;
- Long term cyclization.

Besides all these activities, the “Battery Technology” group also makes tests and characterizes not only the self-fabricated batteries but also commercial batteries.

1.2 Background and project presentation

During the last past years, the world have been trying to find solutions for the likely shortage and the environmental problems related to fossil fuels. The transportation sector is a large consumer of fossil fuels and contributes widely to global greenhouse gas emissions. These emissions could be reduced by substitution of fossil fuels. Full electric cars (energy provided by battery) can achieve zero emission potential if the electricity is produced by renewable energy sources. For these reason one of the main focuses has fallen on renewable energies such solar, wind and wave. However, the batteries that have been used in electrical vehicles, mainly Li-ion, present also several limitations. For this reason, others alternatives have been searched and lithium-sulfur batteries seems to be a promising candidate for energy storage. They offer a higher specific energy (2500 Wh/kg) than Li-ion batteries (200 Wh/kg) and high theoretical capacity (1675 Ah/kg). However, these batteries still suffer from much lower realized capacity and life cycle. The degradation processes, new technologies and materials must be investigated in order to improve the lithium-sulfur batteries performance.

During this work, the morphological changes occurring in the batteries components during their operation were investigated by means of several techniques such TGA, DSC, MS, SEM and XRD. The influence of $LiNO_3$ as additive was also study, as well as the influence of the C-rate in discharge-capacity. Further, two intermediate layers were tested over the cathode in order to avoid the passage of sulfur particles to the anode side.

1.3 Contributions of the work

This research contributes to the investigation of Li-S batteries in following areas:

- Application of TGA, DSC and MS for cathodes analysis of Li-S, quantification of the electrode components and study of its degradation
- Morphological changes of the cathode during cycling observing its surface by means of several techniques
- Influence of intermediate layers placed over the cathode.

1.4 Thesis Organization

This thesis is organized in five main chapters:

- Chapter 1 is the presentation of the work, summarizing the objectives and results of the project as well as a description of the host institution.
- Chapter 2 is an introduction to Li-S batteries including its advantages and challenges that need to be overcome. Some recent researches are also described as well as several techniques used for batteries characterization.
- Chapter 3 describes all the experimental work procedures including the materials, equipment and methods used.
- Chapter 4 presents the results and discussion of the experimental work.
- Chapter 5 is the conclusions chapter that summarizes the results and presents some suggestions for the future.

2. State of the art

2.1 Lithium-Sulfur battery

Among all the available electrical energy storage systems, lithium ion batteries remain the best solution for several applications such as smart-phones and laptops, having a strong influence on their portability, confidence and performance. However, the lithium ion battery is not enough to support higher energy needs like advanced transportation and residential applications. Therefore, new energy storage with higher specific capacity and better performance in their life cycle must be developed. Diverse batteries concepts and different materials have been considered for new application fields such as electric vehicles. Lithium sulfur (Li-S) batteries are one of most promising kind of batteries to be used in the future. According to the complete reduction from elemental sulfur (S_8) to lithium sulfide (Li_2S), sulfur is expected to deliver a specific capacity of 1675 Ah/kg and an energy density of 2600 Wh/kg, which are 3-5 times higher than Li-ion batteries. Li-S batteries have other benefits such as natural abundance of sulfur, low cost, environmental friendliness, wide temperature range of operation, intrinsic protection mechanism against overcharge, low weight and possibility of long cycling. It is also known that Li-S batteries do not suffer from memory effect and that they are very tolerant to overcharging.

2.1.1 Operating Principles

The cathode of Li-S battery is composed by sulfur mixed with a high electrical conductive material, due to the isolating property of sulfur. The anode is normally lithium metal but it is also possible to use different lithium containing materials, such as lithium alloys and lithium deposited into a substrate. Between these two electrodes there is a separator, which is a porous and non-conductive membrane permeable to ionic flow that prevents electric contact between the electrodes. Its main function is to keep the positive and negative electrodes apart from each other to prevent electrical short circuits. Moreover, it allows fast ion transport which is needed to complete the circuit in the chemical cell. An organic non-aqueous electrolyte is normally used to transport and store the ions and it is impregnated in the separator. It is fundamental that the electrolyte does not react with the electrodes and that it is also non-conductive to avoid short circuit between the anode and the cathode [1].

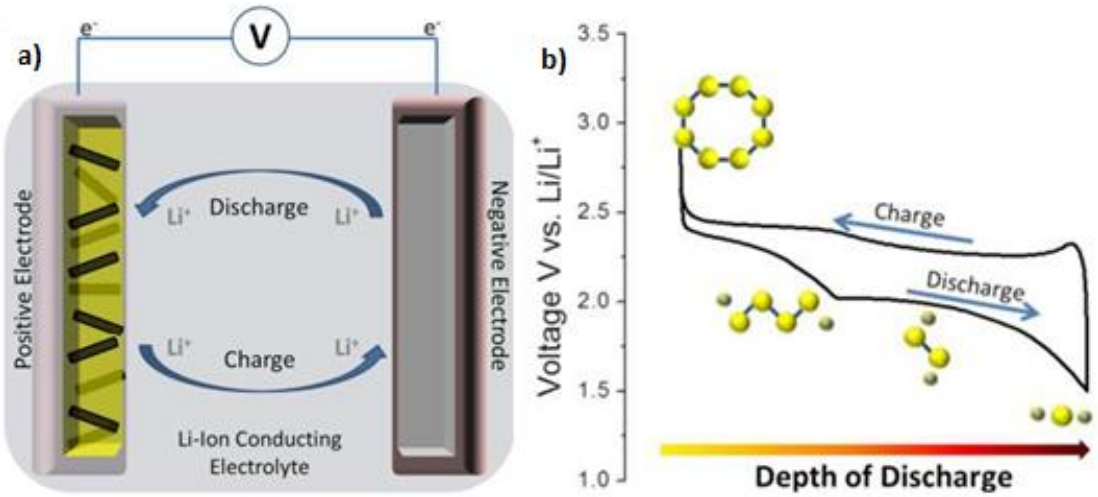

Figure 1: a) Schematic illustration of a typical Li-S cell. The cathode consists of sulfur (yellow) and carbon (black) as a conductive additive separated from lithium (gray) by the electrolyte. b) Typical voltage vs capacity plot for a Li-S cell [2].

The principles of Li-S batteries operation can be explained as follows. During discharge, lithium ions move spontaneously over the electrolyte from the lithium electrode to the sulfur electrode. While this occurs, electrons flow through the external circuit, producing electrical energy. During charge, the lithium ions and the electrons are forced to return in the contrary direction due to an external voltage [3]. On the anode side sulfur is reduced during discharge to Li_2S and oxidized back during charge.

As described before, Li-S batteries have several advantages; however it is known that they have also some limitations to be overcome. These batteries suffer from much lower realized capacity and life cycle. That can be explained through some theories; one of them is the formation/dissolution of polysulfides and their high mobility in liquid electrolytes. The solubility and transport properties of lithium polysulfides in the electrolyte can considerably influence the electrochemical utilization of sulfur, rate capacity and life cycle of these cells. Another problem is the insulating nature of sulfur and Li_2S, the poor intrinsic conductivity (5×10^{-30} S/cm at 25°C) of sulfur which often leads to low electrochemical utilization and limited rate capability requiring contact with conductive materials. The volume/morphology change of the electrode during the cycling is also problematic and it must be improved because it clearly affects the performance of the battery.

The polysulfides shuttle between negative and positive electrodes during the cycling has also an important influence in the battery performance. The polysulfides (PS) at the positive electrode (with a higher order than the ones at the negative electrode) can diffuse to the negative electrode and undergo chemical reactions with lithium to form low-order PS and even insoluble Li_2S_2 or Li_2S if the lithium metal electrode is not protected.

2.1.2 Electrochemical reactions

During charge and discharge a Li-S battery, lithium polysulfides (Li_2S_x) are formed as intermediates, where x=1-8. Polysulfides with a short-chain (x=1-2) are insoluble in the electrolyte, whereas PS with more than two sulfur atoms are soluble in many dipolar aprotic solvents. The electrochemistry occurring at the positive electrode is very complex because of the phase transformations of sulfur that occur during cell operation. The reactions and the typical charge and discharge voltage profile for the first cycle of a Li-S battery are described below. It is possible to divide the discharge process into four regions (see Figure 2). During the first one, the reduction of the dissolved sulfur S_8 to Li_2S_8 occurs, leading to the first upper voltage plateau at 2.2-2.3V (eq.1).

$$2Li + S_8 \rightarrow Li_2S_8 \quad \text{(Eq. 1)}$$

$$Li_2S_8 + 2Li \rightarrow Li_2S_{8-n} + Li_2S_n \quad \text{(Eq. 2)}$$

$$2Li_2S_n + (2n-4)Li \rightarrow nLi_2S_2 \quad \text{(Eq. 3)}$$

$$Li_2S_n + (2n-2)Li \rightarrow nLi_2S \quad \text{(Eq. 4)}$$

$$Li_2S_2 + 2Li \rightarrow 2Li_2S \quad \text{(Eq. 5)}$$

The second region shows the reduction from the dissolved Li_2S_8 to low order PS (eq. 2), during which the cell´s voltage abruptly declines. These two first regions have the highest redox shuttle. In the region III it is possible to find two phases (liquid and solid) from the dissolved PS to insoluble Li_2S or Li_2S_2 (eq. 3-4). The plateau formed at 1.9-2.1 V is responsible for the increase of capacity during the Li-S cells operation. The section IV shows a solid-solid reduction from insoluble Li_2S_2 to Li_2S (eq. 5). This process is kinetically slow and usually suffers from high polarization due to the non-conductive and insoluble nature of Li_2S or Li_2S_2. The insoluble Li_2S is believed to deposit and accumulate at the cathode surface, causing fading as the discharge cycles are repeated even with cycling at less than 50% utilization level [4].

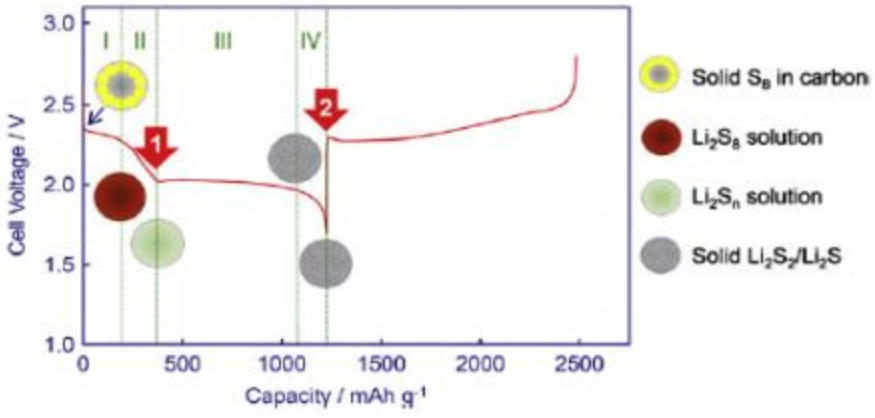

Figure 2: Typical discharge and charge voltage profile of the first cycle of Li/S cells [4].

Normally, the voltage of both discharge and charge shows a small peak, as indicate the two arrows in Figure 2. The first one is the point at which the PS solution has the highest viscosity as a combined result of the S-S chain length and number (concentration) of PS anions. The arrow 2 corresponds to a reduced polarization as a result of the phase transition from the solid Li_2S_2 and Li_2S to the dissolved PS. Upon charge, these to compounds are oxidized into the soluble PS which dissolves into the liquid electrolyte leading to a reduction in the cell´s polarization.

2.1.3 Degradation

To understand what origins degradation and the consequent capacity loss in batteries, some phenomena have to be analyzed. The insulating discharge product (Li_2S) oxidizes to PS during the charge process. However, some Li_2S may not react further and stay at the fully charged state. These agglomerates of residual Li_2S and Li_2S_2 are formed on the surface of cathode with increasing cycle. Some investigations confirmed that the electrode surfaces become less conductive as cycling proceeds [5]. Furthermore, the formation of isolating films block the pores of the cathode upon cycling, so the electrolyte cannot penetrate properly inside the cathode structure limiting the Li^+ ion diffusion and affecting electrochemical reactions and resulting in capacity degradation.

One of the possible explanations is related with the discharge process. While it happens, elemental sulfur (S_8) is first broken to form a chain-structural polysulfide anion (S_8^{2-}), which then combines with Li^+ yielding to high order lithium PS (Li_2S_x, $x \geq 4$) form. Since these PS are soluble in the organic electrolytes, the viscosity of the electrolyte increases. This leads to a decrease of the penetration and diffusion of the Li^+ ion into the inner parts of the cathode and then, most of the reduction reactions take place on the surface of the cathode [6].

Morphological changes occur in the cathode due to the phase changes during the electrochemical reactions. The binder has a considerable influence on the stability of the cathode structure. As sulfur is electrically insulating, the cathodes need an electrically conductive material such as carbon particles. The structure of the positive electrode must allow the electrolyte solution to penetrate for the electrochemical redox reaction take place. That is why several fabrication methods for improving the performance of sulfur cathodes have been tested in recent years.

The discharge and charge processes are widely affected by the polysulfide shuttle phenomenon and it is important to understand that this is related not only to the sulfur electrode but also to the lithium electrode and the electrolyte. If the polysulfide shuttle occurs, it can result in a fast capacity fading and a reduction of the charge/discharge efficiency of Li-S cells (mainly at the high voltage plateau) and can also induce fast self-

discharge. The rapid reduction of the high voltage plateau capacity is associated with high chemical reactivity of high-order PS anions with lithium metal. The capacity decline at the low-voltage plateau is a result of the degradation of the electrodes structure and the precipitation of the insoluble Li_2S on the surface of both electrodes [7].

2.1.4 New concepts

Since lithium sulfur batteries are one of the most promising options to solve the needs of new fields of application like electric vehicles, they have been largely investigated in the last few decades. Their theoretical capacity makes these batteries a very interesting challenge to develop in the next coming years and that can be done improving the chemical and physical properties of their components. It is possible to raise the performance of some components of the battery like the cathode, electrolyte, the lithium or even the separator. Some investigations related to the improvement of these batteries are presented below.

2.1.4.1 Cathode

In order to reach the ideal sulfur electrode several sulfur-carbon composites have been tested. The target is to maintain the structural integrity of this electrode during the cell operation, namely a high porosity and a homogeneous distribution of sulfur. The passage of lithium ions through the cathode must not be blocked and a good electrical connection to facilitate electron transport must be maintained.

Recently, Nazar and coworkers reported that the addition of meso-porous carbon (CMK-3) to highly order composited of sulfur can achieve high reversible capacity with good cycling performance achieving an initial discharge capacity of 1320 Ah/kg after linking the carbon surface with polyethylene glycol to further trap polysulfides [9]. This meso-porous carbon with constraint sulfur inside their channels produces intimate electrical contact. The electrical conductivity of carbon-sulfur composites remain the same even after heat treatment because sulfur is still lodged on the meso-porous channels and do not coat the external surface. Moreover, this framework inhibits the polysulfide diffusion.

Another study is related with a low-cost and environmentally benign chemical reaction-deposition strategy to immobilize sulfur on quasi-two dimensional graphene oxide (GO) [10]. It provides intimate contact between sulfur and carbon. During the heat treatment of the GO-S nano-composites, the bulk sulfur melts and can diffuse through the GO pores. While this happens, this process can partially remove and/or chemically change various functional groups on GO surface improving their conductivity. At the beginning it can lodge volume changes of sulfur when it is converted to Li_2S and back to sulfur. Furthermore, it is possible to create more intimate electronic contact with the sulfur, to avoid agglomeration and loss of electrical contact from the current collector during operation. Although GO-S composite

electrodes improve the cell performance with a reversible capacity of ~900 Ah/kg at 0.1C after 50 cycles, their rate capability is not enough to be used for high-power systems [3].

A recent technique consisting in porous hollow carbon-sulfur composites, exhibited an excellent rate capability results. This method encapsulates sulfur inside a porous shell by vapor-phase infusion and it showed a discharge capacity of 1071 $mAhg^{-1}$ at 0.5 C and 91% of capacity retention after 100 cycles [9].

The effect of a graphitized carbon layer was also investigated. Disordered carbon nanotubes (DCNTs) were synthesized by a template wetting method that uses anodic aluminum oxide membranes [11]. The discharge capacity up to 100 cycles is shown in Figure 3.

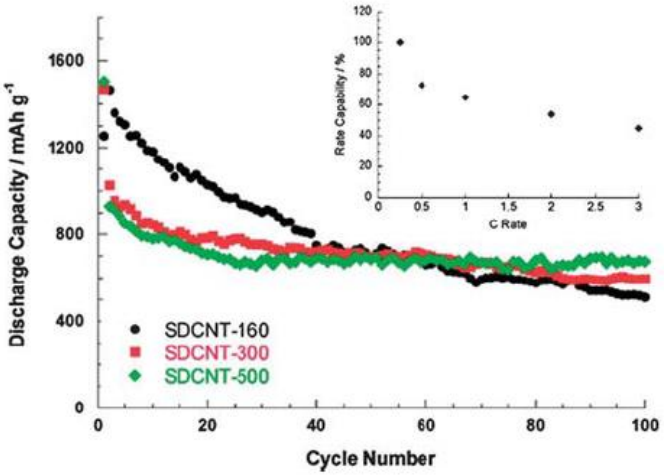

Figure 3: Cycling stability as positive electrodes of Li/S cells. The numbers (160 , 300, and 500) represent the heat-treatment temperature in °C [3].

The binder plays an important role for creating a good electric network structure between sulfur and carbon so that the integrity of the electrode during the cell´s operation is kept. The most common binders are polyethylene oxide (PEO) and polyvinylidene fluoride (PVDF) but other materials have been tested. For example, gelatin has recently been investigated as a binder exhibiting a higher initial capacity and better cycling performance comparing with PEO binder [12].

2.1.4.2 Anode

Some soluble PS can corrode the lithium electrode because polysulfide shuttle phenomenon occurs in this electrode leading to capacity fading and high cell resistance. In order to avoid this problem protected lithium metal electrodes have been developed. The influence of $LiNO_3$ in the electrolyte was studied and it showed that the addiction of this composite can prevent chemical reactions of polysulfides in the electrolyte with the reactive lithium electrodes. A new theory of protected lithium electrodes was investigated related with water-stable NACISON-type Li-conducting ceramic electrolyte with interlayer blocking reactions

between the lithium electrode and solid electrolytes. It is expectable that this protected lithium electrode can increase the cycle life of Li-S batteries [13].

2.1.4.3 Electrolyte

In order to reach a successful performance of the active material in Li-S cells it is important to make a good selection of the suitable electrolyte because of the changes in the solubility of the several polysulfides in the electrolyte and the multi-step reduction reactions of sulfur. For this reason, different types of electrolytes have been tested in Li-S batteries. The requirements for the electrolyte of Li-S battery are electrochemical stability, chemical stability against lithium, ionic conductivity, moderate polysulfide solubility, low viscosity and safety [3]. Some electrolytes are included in systems based on organic solvents such as the carbonate systems, tetrahydrofuran (THF), dimethoxy ethane (DME), 1,3-dioxolane (DIOX), tri(ethylene glycol) dimethyl ether, tetraethylene glycol dimethyl ether (TEGDME), solid polymer electrolytes based on polyethylene oxide (PEO), gel polymer based on PEO and polyvinylidene diflouride (PVDF). However, it is very common that a single organic solvent does not reach all the needs of an electrolyte in a Li-S cell. So, to overcome these limitations, some tests based on a mixture of solvents such as TEGDME/DIOX, TEGDME/THF and DME/DIOX have been made achieving higher yield. Another option to improve the discharge characteristics of Li-S cells is the addition of small amounts of organic additives. For example, adding 5 vol.% of methyl acetate increases the performance of these batteries at low temperatures. It is also known that toluene added to TEGDME solvent could increase the yield of Li-S cells but its quantity was not optimized [19]. In the graphics presented below is possible to see some results of electrolytes tests that have been made to improve the Li-S batteries performance.

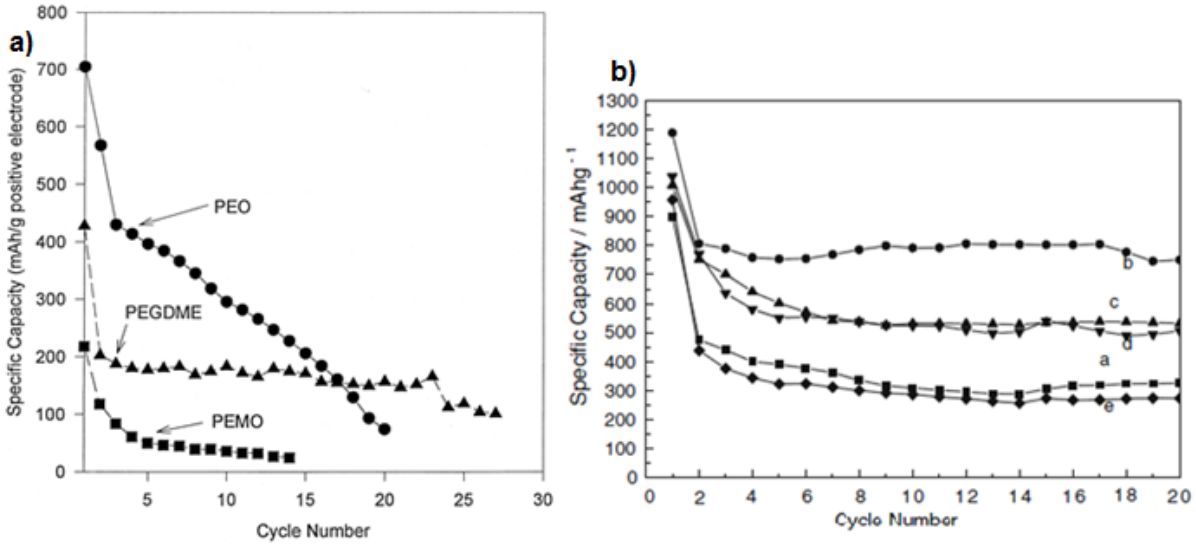

Figure 4: a) Comparison of cycle lives of cells with the three different electrolytes. PEO, PEGDME and PEMO [14]. b) Cycle performance of Li-S battery with different electrolyte composition [DME:DOL = (a) 4:1, (b) 2:1, (c) 1:1, (d) 1:2, and (e) 1:4(v/v)] [15].

Despite PEO has shown the highest first cycle capacity it also exhibited the highest capacity fade (Figure 4a). The PEGDME had a low capacity fade with 0.9%/cycle and the second highest discharge capacity [14]. In the second test (Figure 4b) the best cycle performance, the highest initial discharge capacity and the lowest fading rate were obtained with the electrolyte of DME:DOL=2:1 (v/v) and after 20 cycles this battery still remained at 750 $mAhg^{-1}$ [15].

Figure 5 shows examples of two different Li-S batteries additives and their performance.

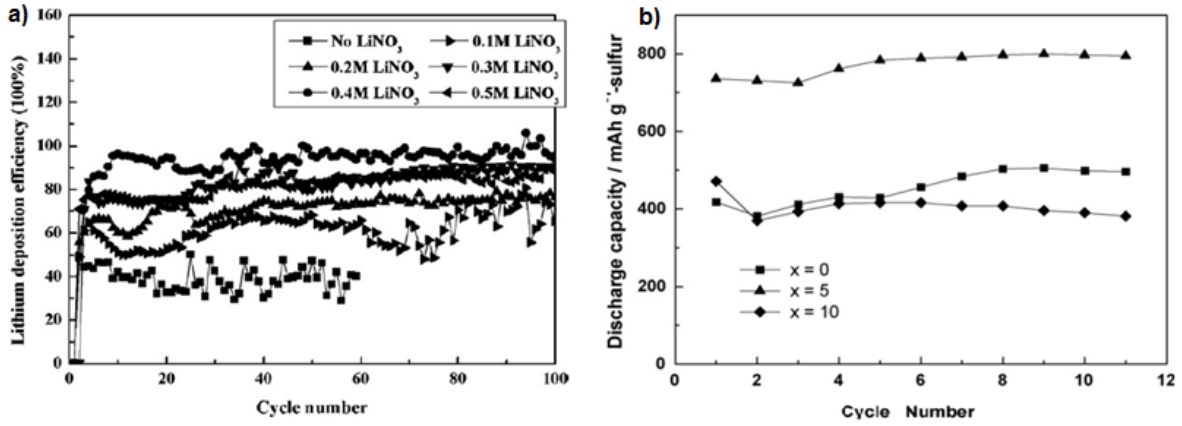

Figure 5: a) Cycling efficiency (EFF) of the lithium deposition and dissolution on the Cu foil in different electrolytes [16]. b) Cycle performance of Li-S cells with 1M $LiCF_3SO_3$ in TEGDME electrolyte containing x% of toluene additive [17].

In Figure 5a it is possible to see that adding $LiNO_3$ to the electrolyte clearly improves the lithium deposition efficiency. The highest cycling efficiency was obtained for 0.4 M $LiNO_3$ [16].

The Figure 5b shows that the initial discharge capacity increases with toluene combination. The highest value was obtained with 5% of toluene addition and this value is 1.8 times higher than the value corresponding to the electrolyte without toluene.

2.2 Characterization techniques for Li-S batteries

In order to characterize the performance and to understand better the reactions and processes occurring before, during and after the Li-S cell´s operation, several techniques can be applied. In this chapter, some of these techniques will be summarized.

2.2.1 Scanning Electron Microscope (SEM)

Scanning electron microscope uses a focused beam of high-energy electrons to generate a variety of signs at the surface of solid samples. These electrons interact with electrons in the material sample, creating numerous signals that can be detected. The information about the sample's surface morphology, chemical composition and crystalline structure is then obtained. This kind of microscope can reach resolutions of 1 nanometer.

The back scattered electron and the secondary electron are two types of signals produced by a SEM. The first one is the reflection of waves, particles or signals back to the direction from which they came. Its operation is similar with a mirror, it is a diffuse reflection due to scattering, as opposed to specular reflection. On the secondary electron the electrons are generated as ionization products, they are created by other radiation that can appear in form of ions, electrons or photons [18].

2.2.2 Atomic Force Microscopy (AFM)

AFM or scanning force microscopy (SFM) is also a microscopy technique with a very high-resolution. The demonstrated resolution is on the order of fractions of a nanometer, 1000 times better than the optical diffraction limit. The AFM offers a three-dimensional surface profile while the one provided by SEM is only two-dimensional. However, it is important to notice that the SEM can reflect an area on the order of square millimeters with a depth of field on the order of millimeters, while the AFM can only reflect a maximum height on the order of 10-20 micrometers and a maximum scanning area of about 150×150 micrometers. This technique is applied in Li-S batteries for investigating the formation of isolating layers and the distribution of sulfur particles over the surface.

2.2.3 X-Ray Diffraction

The X-ray diffraction is a typical technique to study crystal structures and atomic spacing. It involves three basic elements: an X-ray tube, a sample holder and an X-ray detector. The X-rays are produced in a cathode ray tube by heating a filament to generate electrons, accelerating the electrons toward a mark by applying a voltage then the target material is bombarded with electrons. If the electrons achieve enough energy to dislodge inner shell electrons of the target material and the corresponding X-ray spectra are produced [19].

2.2.4 Raman spectroscopy

Raman spectroscopy is a technique centered on inelastic scattering of monochromatic light, typically from a laser source. After being absorbed, the photos of the laser light are reemitted. This laser interacts with molecular vibrations resulting in the energy of the laser photos being shifted up or down, and then the shift in energy gives information about the vibrational modes in the system [20]. Raman has been also used for the investigation of the intermediates products (polysulfides) of Li-S batteries.

2.2.5 Simultaneous Thermal Analysis (STA)

Simultaneous Thermogravimetry - Differential Scanning Calorimetry TG-DSC measures both heat flow and weight changes in a material as a function of temperature or time in a controlled atmosphere. Simultaneous measurement of these two material properties not only improves productivity but also simplifies interpretation of the results. The complimentary information obtained allows differentiation between endothermic and exothermic events which have no associated weight loss (e.g., melting and crystallization) and those which involve a weight loss (e.g., degradation).

2.2.5.1 Thermogravimetric Analysis (TGA)

Thermogravimetric analysis or thermal gravimetric analysis is a very useful technique to measure the amount and rate of change in the weight of a material as a function of temperature or time in a controlled atmosphere. With this equipment it is possible to characterize materials that exhibit weight loss or gain due to decomposition, oxidation or dehydration. This technique can measure the composition of multicomponent systems, the thermal and the oxidative stability and the decomposition kinetics of materials, the effect of reactive or corrosive atmospheres on materials, moisture and volatiles content of materials and estimate the lifetime of a product.

2.2.5.2 Differential Scanning Calorimetry (DSC) /Differential Thermal Analysis (DTA)

These two techniques are used to measure endothermic and exothermic transitions as function of temperature. This equipment is used to characterize polymers, organic and inorganic chemicals. Transitions measured include glass transitions, crystallization, melting and sublimation [21]. Usually two thermocouples are used to work with this technique, one always empty as reference and the other to hold the sample. The difference in the amount of heat absorbed to increase the temperature of a sample and reference is measures as function of temperature.

2.2.6 Mass Spectrometry (MS)

Mass spectrometry is a technique used to determine the elemental composition of a sample, the masses of particles and molecules, and to elucidate the chemical structures of molecules. It displays the spectra of the masses of the molecules comprising a sample of material. The mass spectrometer consists of three components: ion source, mass analyzer and detector. The spectrometer ionize the chemical compounds, these ions are extracted into the analyzer region of the mass spectrometer where they are separated according with their mass to charge ratios. The ions are detected by a mechanism capable of detecting charged particles. Then this signal is sent to a data system where the ratios are stored

together with their relative abundance for presentation in the format of ratios spectrum. This technique is able to work simultaneously with other equipment, for example TGA [21].

2.2.7 Ultraviolet-Visible Spectroscopy (UV-spectroscopy)

Ultraviolet–visible spectroscopy (UV) is a method used to define which wavelengths (colors) of visible light a sample absorbs or emits. Frequently, when molecules absorb light, they are placed into a higher energy level which is less stable than their ground state. When the molecules return to their ground state, they release light with wavelength equal to the one previously absorbed. The main difference between the light that is emitted and the light that was absorbed is the direction. Since the emitted light can be released in any direction and in order to avoid measuring light from the source, rather than simply measuring the light that has been emitted, detectors in emission spectroscopy are often put at a 90 degree angle from the source light beam [22].

This method can be used to study the reactions occurring in Li-S batteries identifying the different polysulfides present during the battery operation.

3. Experimental Work

3.1 Battery Preparation

3.1.1 Cathode

3.1.1.1 Composition

The experimental work began with the preparation of the suspension for the cathode. Carbon black (Super P® Conductive, Alfa Aesar 99%) that has a high electrical conductivity was mixed with sulfur (Sigma Aldrich, 99.98%) in order to improve the electrical conductivity of the cathode since sulfur has a low electrical conductivity. Polyvinylidene fluoride (PVDF, Sigma Aldrich) was dissolved in Ethanol Absolut (Th.Geyer Chem Solute) and dimethylsulfoxide (DMSO, VWR ProLab, 99.6%). PVDF is the binder to maintain in contact the particles of carbon black and sulfur. Due to the high resistance of this plastic material brings stability to the cathode layer. DMSO was added in order to dissolve PVDF because it is a polar aprotic solvent that dissolves in polar and nonpolar compounds and it is also miscible in a wide range of organic solvents. The addition of ethanol accelerates the drying process because of its high volatility.

The composition of the suspension prepared at the beginning of the experimental work is presented in the Table 1.

Table 1: Composition of the cathodes suspension.

S	CB	PVDF	Ethanol	DMSO
wt.%	wt.%	wt.%	wt.%	wt.%
50 %	40 %	10 %	50 %	50 %

3.1.1.2 Mixture

The mechanical mixing of the suspension was made in a tumbling mixer. Some ceramic spheres were put inside the tumbling in order to increase the collisions between the particles and to eliminate the agglomerates in the suspension. Carbon black powder and sulfur were mixed together in the tumbling mixer during one day to obtain a homogeneous suspension. DMSO, ethanol and PVDF were mixed magnetically during 2 hours to achieve a good dissolution of the PVDF. At the end, all the components were mixed together in the tumbling mixer.

3.1.1.3 Spraying

The home-made suspension-spray machine (Figure 6) was used to prepare the cathode. The previously prepared suspension was sprayed over a carbon coated aluminum foil substrate with the aim of obtaining homogenous and thin layers. The recipient containing the

suspension had a magnetic bar inside to avoid agglomeration and solid deposition. It also has to be closed to maintain constant the pressure inside. Connected with this recipient there are two hoses: one for the air feed with the function of creating overpressure in the suspension and the other connected with the mixing nozzle for spraying. Two other air pressure hoses are connected to the nozzle; one for opening and closing the entrance of suspension (by means of a needle movement) and the other connected for air feed, making it is possible to regulate the air pressure for spraying. This machine can work with several programs and it is possible to change the speed and the axes of the operation. The optimal spraying conditions found were 0.4-0.5 bar for the air pressure and 0.2-0.4 bar for the suspension overpressure. Each substrate has been sprayed with 3-4 layers and after spraying each one of them was dried in the oven at 60ºC.

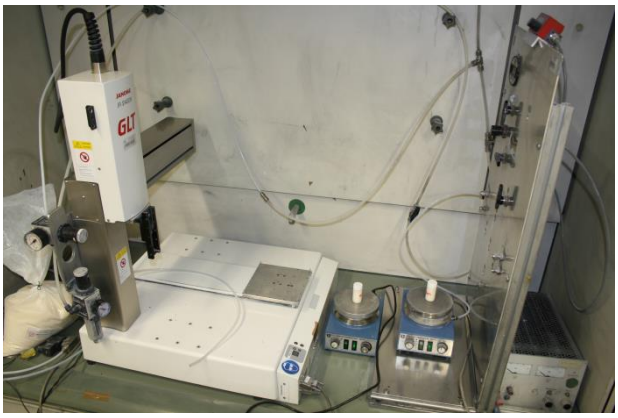

Figure 6: Home-made suspension-spray machine.

3.1.2 Electrolytes

The electrolytes were prepared inside the glove box under Argon atmosphere (Figure 7), with negligible quantities of O_2 and H_2O (2-8 ppm). This avoids the reactions that could occur due to the high reactivity of lithium and electrolyte components in contact with air and water.

Two electrolytes with different composition were used (Table 2). They are composed with the same common used lithium salt: hexafluorophosphate ($LiPF_6$, Alfa Aesar, 99.99%). E_4 had lithium nitrate ($LiNO_3$, Sigma Aldrich) as an additive, which is known for increasing the coulomb efficiency to 100%. The salts were dissolved in tetra(ethylene) glycol dimethyl ether (TEGDME, Sigma Aldrich, 99%).

Table 2: Compositions of the different electrolytes used.

Electrolyte	$LiPF_6$ (M)	$LiNO_3$ (M)
E_0	1	-
E_4	1	0.75

The electrolyte components were mixed in a magnetic stirrer in order to accelerate the dissolution of $LiNO_3$ and $LiPF_6$ in TEGDME.

Figure 7: Glove box used to prepare electrolytes and batteries.

3.1.3 Swagelok Cell

The components of the batteries (cathode, separator, electrolyte and anode) were assembled in a proper cell in the glove box. The cathode was cut from the sprayed cathode by a hollow punch using a hammer and then weighted to estimate the quantity of sulfur in each battery.

The separator used was a monolayer membrane of polypropylene (Celgard 2500), because of its high resistance to most chemicals, uniform structure and high porosity. The separator was cut in the same way as the cathode with a higher diameter size.

A Swagelok Cell (Figure 8b) was used to arrange and maintain the battery hermetic. Two sizes of Swagelok Cell were used, consequently, the sizes of the main components were also different. However, the sequence of placement of the different components was maintained (Figure 8). First, the cathode was placed over the aluminum plate inside the Swagelok cell. Under this aluminum plate there was a compression spring to avoid possible damages in the cathode and relieve the pressure caused when the battery is closed. Next, 14µL of the electrolyte were added over the middle of the cathode, and then the separator was placed on top of it. The lithium metal was placed over the separator (Figure 9) and the battery was finally closed and tightened with a screwdriver. The open circuit voltage (OCV) measured after building varied usually between 2.5-3.5V.

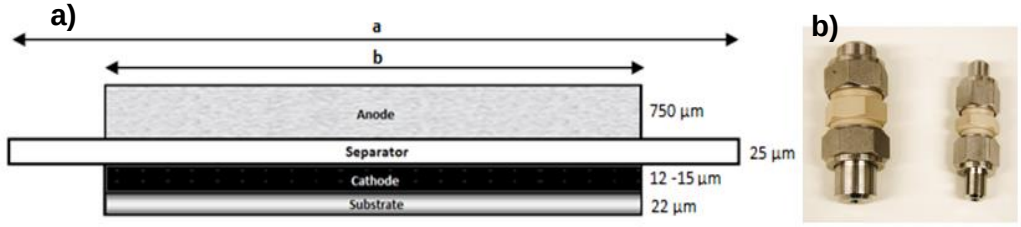

Figure 8: a) Sequence of the components in the battery and their thickness. b) Swagelok Cells. Big batteries: a-22 mm and b-16 mm. Small batteries: a-12 mm and b-10 mm.

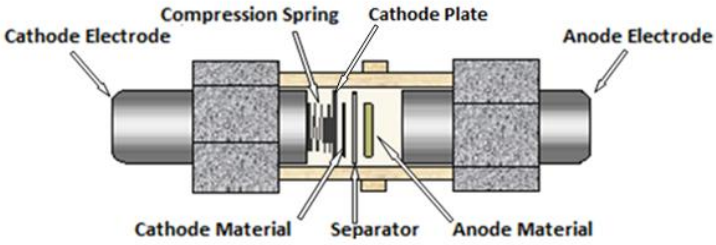

Figure 9: Representation of the Swagelok Cell.

3.1.4 Intermediate layers

With the purpose of lodging the sulfur particles on the cathode during the cell operation, which would avoid their passage to the other side of the separator, two intermediate layers were tested. The first one was a micro-porous carbon diffusion layer (CDL) (SGL25BA) (Figure 10) being the procedure very similar to the one described above. The smallest batteries were chosen for this experiment. The main changes were the deposition of the CDL over the cathode and the quantity of the electrolyte added, this time 42 µL of E4 have been placed (14 µL over the cathode, 14 µL over the CDL and 14 µL over the separator).

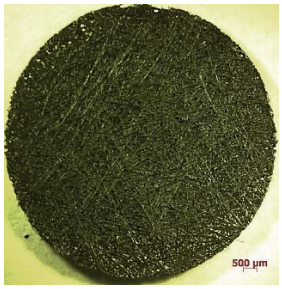

Figure 10: Carbon diffusion layer.

In the second test, a nano-porous layer composed by carbon black and PVDF was sprayed over the surface of the simple cathode (SC). The final composition of this cathode (SC: +CB) can be seen in Table 3.

Table 3: Composition of a simple cathode and the final composition of the cathode with an extra layer.

Cathode	S	CB	PVDF	Ethanol	DMSO
	wt.%	wt.%	wt.%	wt.%	wt.%
SC	50	40	10	50	50
SC: +CB	33	57	10	50	50

3.2 Battery cycling

The batteries were analyzed in a battery tester (BaSyTec) (Figure 11). The tester had 16 channels which allow testing 16 batteries simultaneously. Its system permits to program a plan for each test. Each plan contained all the parameters intended for the cycling like the

current intensity, the potential for charging and discharging or the number of cycles. To assure that the battery is completely charged before starting the discharge, the potential for charging was maintained at 2.8 V until the current decrease to 1/3 of the charge current or after 15min of potentiostatic charge (potential is maintained constant). For security reasons, a maximum and minimum voltage were set, and the program would shut off if the battery reached theses values. The program would also stop the measure in case the temperature reaches values higher than 80°C. After finish the plan, it is possible to get the values of the discharge, charge curves and the variation of the specific capacity. Capacity is the total Amp-hours available when the battery is discharged at a certain discharge current from the 100% state-of-charge to cut-off voltage [23]. If this capacity were divided by the weight of the sulfur present in the cathode it will be obtained the specific capacity (Ah/kg_{Sulfur}). The efficiency of the battery is an important issue that can be evaluated calculating the Coulombic Efficiency. This efficiency is the ratio of the number of charges that enter the battery during charging compared to the same number belonging to the discharge.

One of the parameters studied during this experimental work was the C-rate capacity. This concept refers to a unit to declare a current value which is used for estimating the effective time of battery variable charge/discharge condition. This means that operating with 1 C-rate the discharge current will discharge the entire battery in one hour.

Figure 11: Batteries testing in BaSyTec equipment.

3.3 Microscopic and spectroscopic characterization

3.3.1 Electronic microscopy

For security reasons, the next step (disassembling of the battery) was performed in the hotte. The objective was to take the cathode and the separator out of the battery, and try not to damage their surface during this process. Then they were placed in the oven in order to evaporate the electrolyte. Next, the electronic microscope Zeiss Cam ICc3 was used to take pictures with 6.5 - 50 of range resolution. The pictures were taken over the entire active surface of the cathode and over both sides of the separator, using different magnifications.

The purpose of the pictures was to see the changes of the cathodes before and after cycling, the influence of different electrolytes and cathode layers.

3.3.2 SEM

Some cathodes were characterized with SEM. This technique allowed the observation of nano and micro particles on the cathode surface. With back scattered electron (BSE) it was possible to observe contrasting colors representing different elements for each contrast. For higher mass number, brighter colors are observed. In this experimental work the lighter color belongs to sulfur once it has a mass number of 32 g/mol.

Energy dispersive X-ray spectroscopy (EDX) complemented the BSE information identifying the elements corresponding to each contrast.

3.3.3 XRD

X-Ray diffraction was used in order to characterize the structural properties of the cathode materials. The identification of sulfur and the analysis of its structure was the main focus of the application of this technique. X-ray diffractograms were recorded with an X-ray diffractometer, D8 Discover GADDS, equipped with a VÅNTEC-2000 area detector. The accelerating voltage was 45 kV and the tube current was 0.650 mA. Each diffraction pattern was measured in four frames with a step size of 23°, starting with $\Theta_1=\Theta_2=12°$. The exposure time for each frame was 180 s.

3.3.4 STA and Mass Spectrometry

Simultaneous TG-DTA/DSC-Apparatus (STA) and the mass spectrometer (MS) (MS403C) (Figure 12), both from the company NETZSCH were applied for the identification of mass and energy changes as well as the gas reaction products produced during test.

Figure 12: a) Simultaneous TG-DTA/DSC-Apparatus; b) Mass spectrometry MS403C.

In an initial phase of this work, only the STA equipment was used. This equipment includes two simultaneous applications: the TGA and DTA/DSC methods.

Two sample carriers were used (Figure 13). The sample carriers are position over an arm of a recording microbalance. Figure 13a shows the sample carrier used for carry out measurements in simultaneous TGA/DTA mode. This sample holder contains two crucibles, one always empty as reference, and the other to hold the sample. Both crucibles are made of Pt/Rh (T_{max}=1700°C), have a diameter of 6.8 mm and a volume of 85 µl with Al_2O_3 as coating material for the inside walls. Each crucible is in contact with a thermocouple, these make possible the DTA. The sample carrier was placed in a furnace where the temperature was controlled in a pre-programmed temperature/time profile. The gaseous environment of the sample can also be defined, in this work air and argon were the gases used. The reference crucible stay at the same programmed temperature while the sample crucible temperature may change due to the energy produced or consumed in reaction or transformation process. The gas 1 (coming from the base) was the protective one and it was used to purge the balance chamber. The gas 2 was the gas for the sample holder chamber and it was introduced from the side, directly to the sample region.

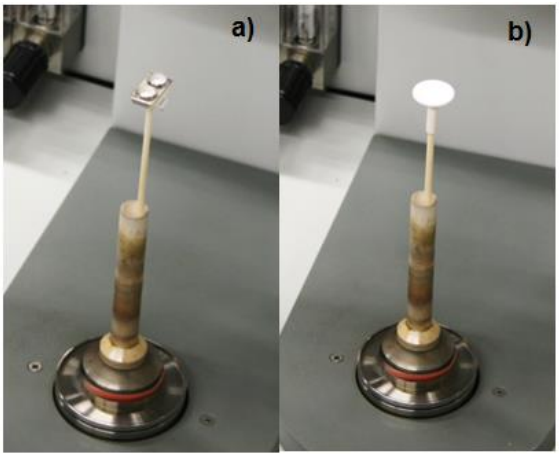

Figure 13: a) Sample carrier with two thermocouples; b) Sample carrier used to work together with the mass spectrometry equipment.

Before start the measurement of the cathodes, their main components (sulfur, PVDF, CB) were individually analyzed under the conditions presented in the Table 4.

Table 4: Conditions used during the STA measurements.

Conditions	Gas 1: Flow rate (mL/min)	Gas 2: Flow rate (mL/min)	Pressure (Bar)	Heating rate (K/min)	Ti (°C)	Tf (°C)
1	**Air** 30	**Air** 30	0.5-1.5	5	35	1000
2	**Argon** 1) 80 (2 h) 2) 30	**Argon** 1) 80 (2 h) 2) 30	0.5-1.5	5	35	1000

After the test is finished, it is possible to get the plot of the mass loss and/or heat required against temperature or time.

The TGA system can be coupled with the mass spectroscopy system analyzing the gases produce in the sample simultaneous with the DSC/TGA measurement. For the measurement of the cathodes it was decided to use a single and larger crucible as sample holder which was connected with one thermocouple (Figure 13b). This thermocouple is made of Al_2O_3 (T_{max}=1700°C) and it has a diameter of 17 mm.

With this crucible, thermogravimetric analysis and mass spectroscopy were performed simultaneously. However it is not possible to obtain the values of energy changes. The advantage of this ceramic plate is that the cathode does not have to be cut, avoiding the possible loss of material during preparation of sample. Only batteries with a cathode diameter of 16 mm were analyzed through this system in order to obtain more precise MS results. During the operation, the spectrometer ionize the chemical compounds, these ions are extracted into the analyzer region of the mass spectrometer where they are separated according with their mass to charge ratios. The ions are detected by a mechanism capable of detecting charged particles. Then this signal is sent to a data system where the ratios are stored together with their relative abundance for presentation in the format of intensity (measured ion current) versus mass number.

The operation conditions were the same as conditions 1 (Table 4). This configuration can display at the same time the plot of “ion current against time or temperature” with the plot of “mass loss against time or temperature”.

4. Results and Discussion

4.1 Battery peformance

4.1.1 Influence if $LiNO_3$ as additive

The influence of $LiNO_3$ as additive in the electrolyte was tested in several batteries. The electrolyte E0 was composed by 1 M of $LiPF_6$ dissolved in TEGDME and E4 had the same composition but 0.75 M of $LiNO_3$ was added. Figure 14 shows the results of two batteries using these electrolytes and operating with 0.2 C-rate. In the additional information (Annex A) the average of the several cycling tests of these batteries are shown.

As can be seen in Figure 14 a) the additive clearly improves the discharge capacity of the battery during the whole cycling presenting more than 600 Ah/kg after 100 cycles, which is 400 Ah/g higher than the batteries using E0, however degradation is present in both cases.

In Figure 14b it is possible to see that the coulombic efficiency curves differ for batteries made with E0 and E4. For batteries with E4, after the first five cycles, the curve stabilizes in values very close to 100% until the end of the test which means that the values of the discharge and charge capacity are very similar. The batteries with E0 present a very instable curve with values under 100%, by other words the shuttle mechanism is not being avoided.

This can support the theory of the formation of a protective film over the anode when $LiNO_3$ is used, which reduces the shuttle mechanism avoiding the concentration of low order polysulfides over the lithium and the consequent loss of capacity.

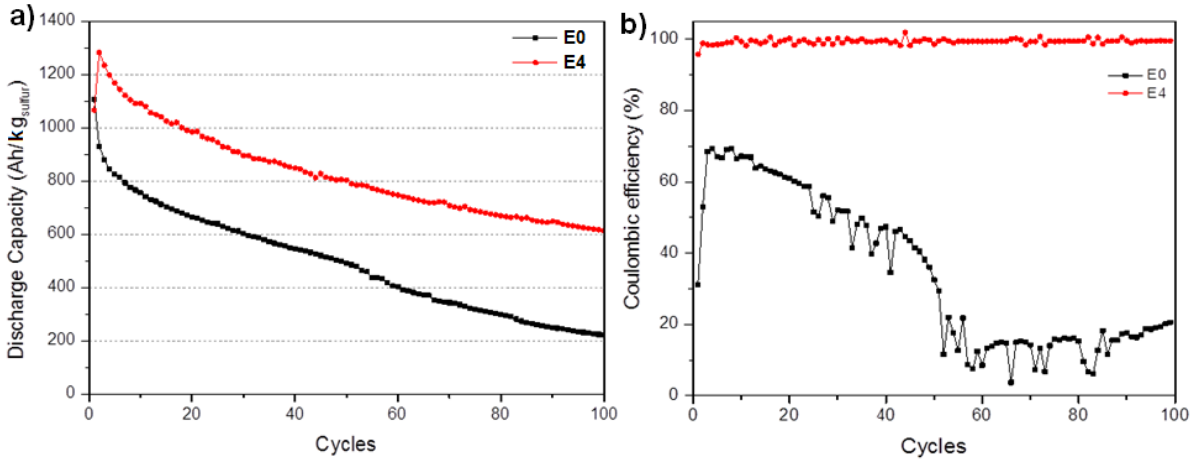

Figure 14: a) Discharge capacity curves for batteries tested with E0 and E4 as electrolyte; b) Charge-discharge efficiency curves.

In order to see the changes in the components of the batteries before and after cycling, microscopic pictures were taken to several cathodes and separators. Sulfur crystals were found on the surface of several separators, mainly on the anode side. The following pictures show the surface of different separators after cycling and using E4 as electrolyte.

Figure 15a shows some black regions which are cathode material introduced in the porous of the separator. Picture c) was taken without removal of the separator from the cathode, so it is possible to see both components in the picture.

Crystals of sulfur appear in all these separators which mean that the high order polysulfides diffused to the anode side, reacted there and the end products and the insoluble polysulfides accumulated over the separator surface. As the pictures show, the quantity of sulfur crystals is higher with increasing number of cycles.

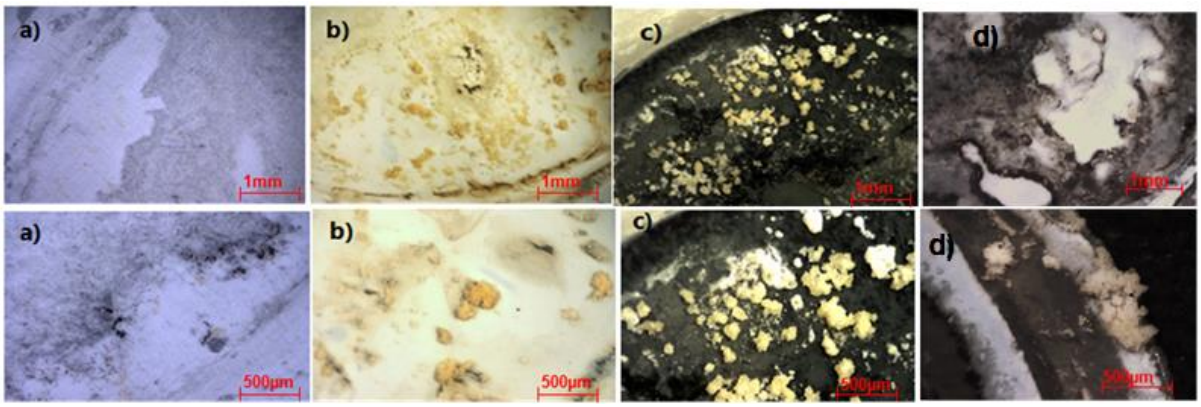

Figure 15: Separators surface (anode side) after cycling and using E4: a) 5, b) 23, c) 100 and d) 100 cycles.

Pictures of the separators from the batteries using E0 as electrolyte were also taken. Figure 16 shows these separators after cycling. The sulfur crystals are observed but in lower quantity and smaller size that in Figure 15. One of the mains differences is the orange color in the surface of the separators with E0. Polysulfides of high order have a red color and may be observed by opening the battery in charge state. Nevertheless, this color was observed by batteries which were already dried. Elemental sulfur is red after melting and fast cooling due the formation of polymeric sulfur. The high charge time required for the formation of sulfur in batteries with E0 may change the structure of sulfur and sulfur may be present in an amorphous state, observed as a red color.

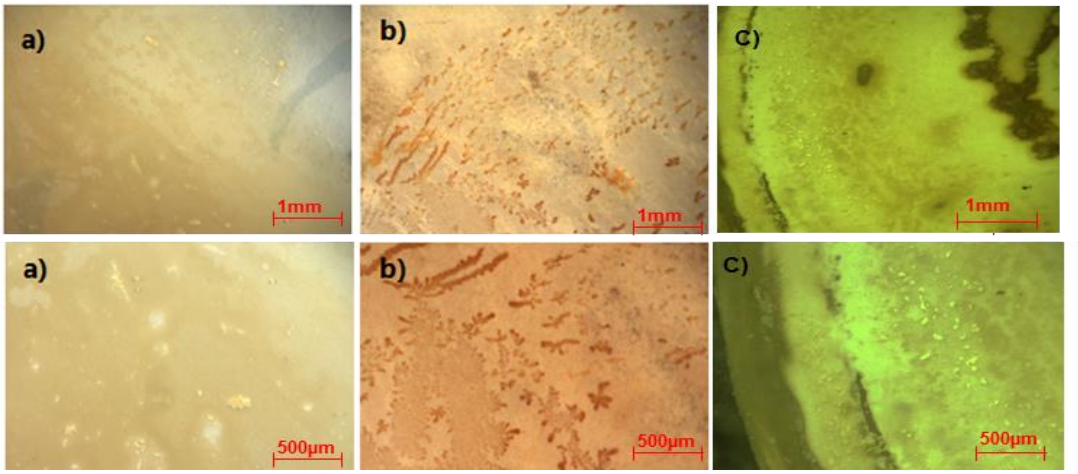

Figure 16: Separators surface (anode side) after different number of cycles and using E0: a) 1 cycles; b) 11 cycles; c) 100 cycles.

Microscopic pictures were taken over several cathodes surfaces in order to see their morphological changes occurring for different number of cycles after operating under 0.2 C-rate (Figure 17). Some pictures show damaged regions, which were caused during the removal of the cathode from the separator. Some cathode material is kept in contact with the separator after remove. The higher resolution pictures were taken over the intact regions.

The image of the cathode before cycling has a homogeneous surface with some shiny points that are sulfur particles. When comparing it with cycled cathodes, it is possible to see that their surfaces change along the cycling. The smallest the number of cycles, the higher quantity of sulfur we can see on the surface of the cathodes. From cycle to cycle, the sulfur particles leave the cathode surface, reaching an almost homogeneous black surface at the 100th cycle. These results are exactly the opposite of the ones obtained by the separators pictures, where the quantity of sulfur increases with the number of cycles. Summing up, is possible to conclude that high order polysulfides diffuse to the anode side, react there forming insoluble polysulfides and end products which accumulate on the separator surface.

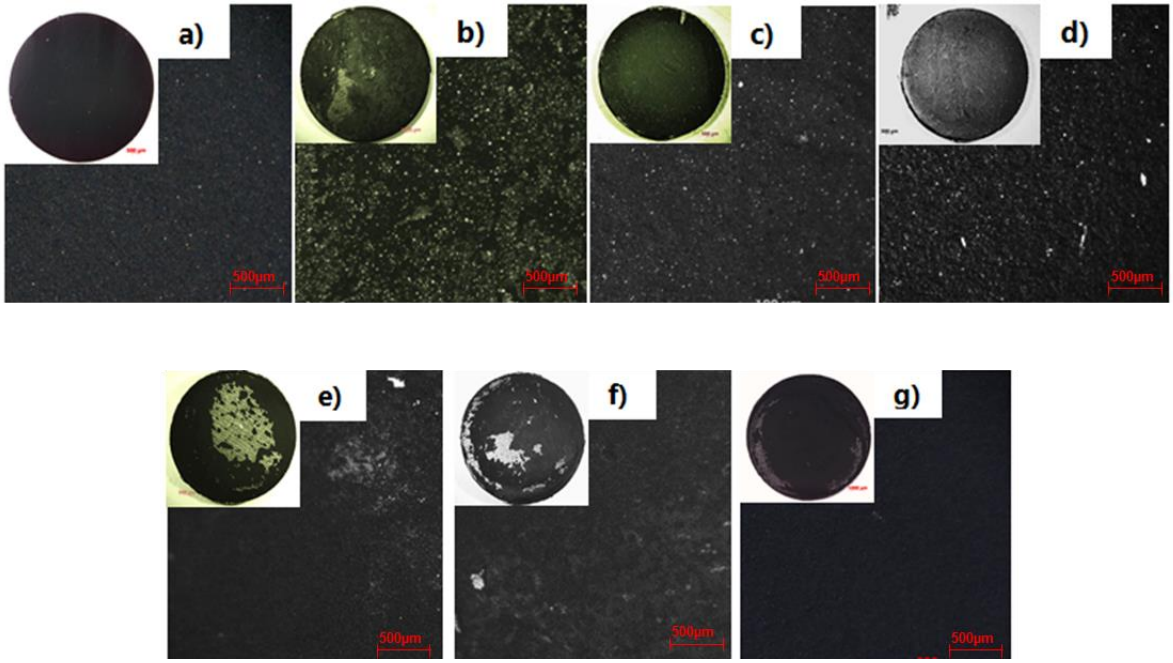

Figure 17: Cathodes surfaces using E4: a) before cycling; b) 1, c) 5, d) 10, e) 25, f) 50 and g) 100 cycles.

Figure 18 shows the SEM images of 3 different cathodes. Figure 18a illustrates a cathode that has the most part of the sulfur particles covered by carbon black. Image b) presents some lighter marks that be may the places where sulfur particles were before and also a few cracks left by the flow out of the sulfur particles confirming their abandonment from these cathode to the separator as already seen. In picture c) there are some lighter regions on the surface which are large agglomerations of sulfur formed during charge of the battery.

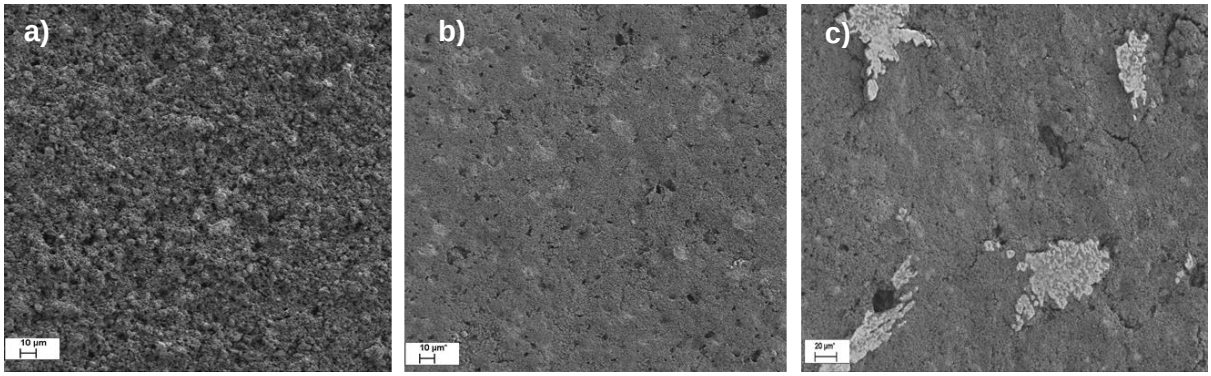

Figure 18: SEM images of cathodes (magnification: 300x): a) before cycling, b) after 100 cycles using E0 as electrolyte and c) after 100 cycles using E4 as electrolyte.

As support of these results, XRD analysis was performed in these three cathodes (Figure 19). The cathode before cycling presents a crystal orthorhombic face-centered structure of sulfur randomly orientated. In cathode using E0 there are no peaks meaning that any crystalline sulfur has been detected. The cathode using E4 shows some peaks with different intensities when compared to the ones of the cathodes before cycling. This is caused by the new orientation of the particles after cycling. These results are in agreement with the SEM images of the Figure 18.

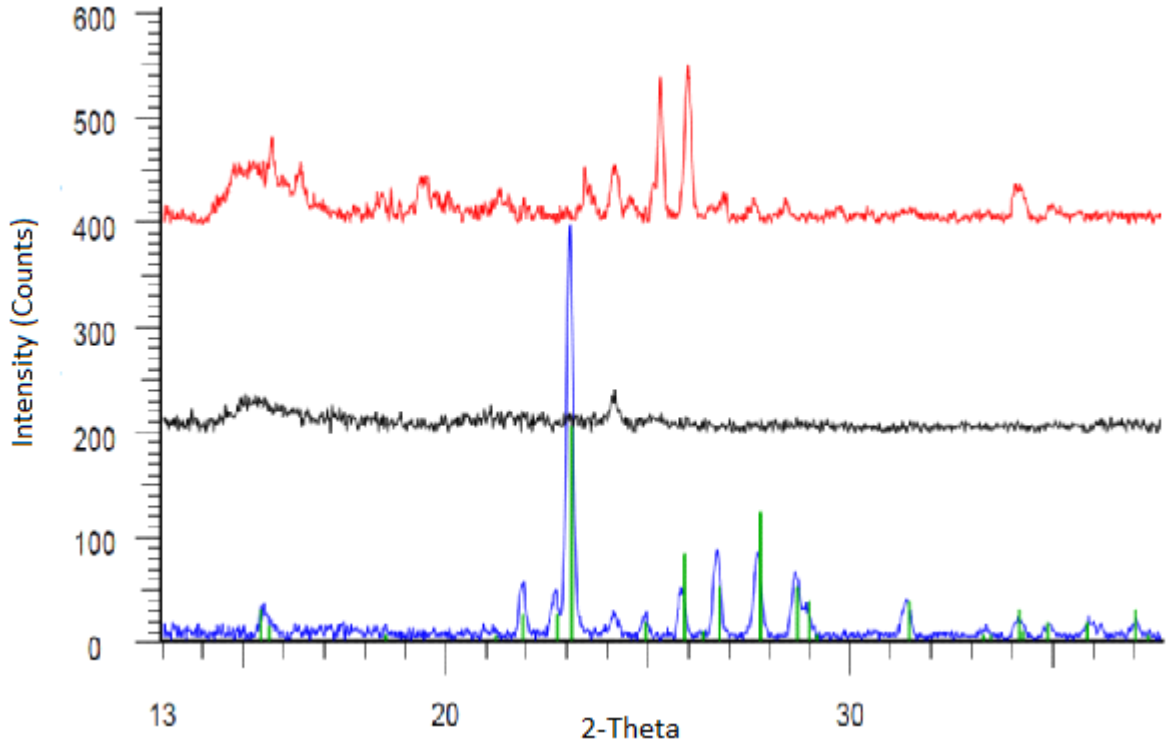

Figure 19: XRD spectra of cathodes: before cycling (blue), after 100 cycles using E0 (black) and using E4 (red). PDF pattern: 00-008-0247 Sulfur (green).

4.1.2 Influence of C-rate on discharge capacity

The influence of the discharge rate in the discharge capacity was investigated for different number of cycles. Figure 20 illustrates these results and represents an average of the values obtained from two batteries for each C-rate. The best performance was obtained for 1C-rate which is an intermediate value. The degradation of batteries is higher by cycling at very low C-rate (0.1) and very high C-rate (2 C). The values of the discharge capacity at 2 C-rate are rather constant during cycling; however they are also very low. This low capacity may be explained by incomplete reaction of end products. The high current density hinders the crystallization of Li_2S. On the other hand, with 0.1C-rate the initial capacity is the highest. The low current density allows an almost complete reaction from sulfur to Li_2S. However, it presents also the highest fall of capacity. This may be explained by the presence of higher amount of end isolating products that are formed on the surface of the electrodes. Moreover, at lower cycling current the battery presents and additional self-discharge, which contributes to the loss of capacity.

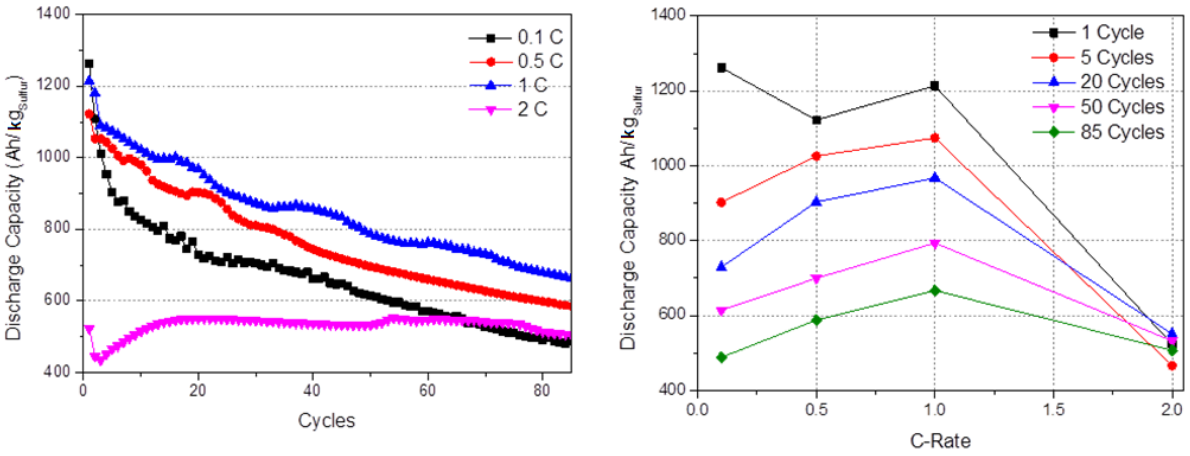

Figure 20: Discharge capacity at different C-rate.

The potential for the first and second plateau for the 1st discharge changes with the C-rate values. As expected, at higher values of C-rate the potential are lower due to the incomplete reduction reactions (Figure 21). At the 85th cycle, the potential of the first plateau is the same for all C-rates. At the second plateau, high discharge current densities lowered the potential of reactions.

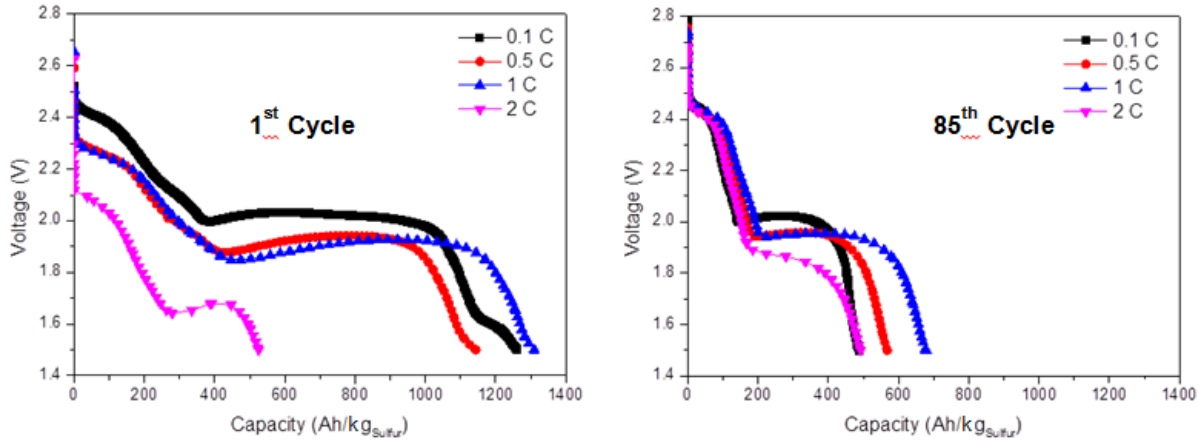

Figure 21: Potential obtained from the 1st and 85th cycles using different C-rate.

4.2 STA and mass spectroscopy of cathodes

4.2.1 Cathode components

The thermal behavior of each battery component was analyzed first separately by STA under different atmosphere.

Figures 22 and 23 show the DSC/TG analyses of sulfur under air and under argon atmosphere, respectively. In Table 5 the phase changes and reaction temperatures, as well as the enthalpies values are described. The peak 1 at 109°C and the peak 2 at 122°C in Figure 22 (blue line) correspond to sulfur melting points. These enthalpies peaks are not related with a change of mass. The theoretical melting point of the elemental sulfur is 115°C. These two temperatures correspond to α and β that are two transition phases in the fusion of the sulfur. The stable standard temperature pressure form of sulfur is orthorhombic α-sulfur consisting of cycloocta-S molecules. Increasing the temperature until 95.3 °C, this phase converts into monoclinic β-sulfur which melts at 119.6 °C (Eq. 6 and 7).

$$\alpha \cdot S_8(s) \rightarrow \text{cyclo} \cdot S_8(l) \qquad \text{(Eq. 6)}$$

$$\beta \cdot S_8(s) \rightarrow \text{cyclo} \cdot S_8(l) \qquad \text{(Eq. 7)}$$

The loss of mass starts at 140°C which means that start to change to the gas phase. At temperatures between 200-1000°C sulfur vapor involves molecules with 2-10 atoms. The peak 3 at 325°C may include the vaporization process, although being an endothermic reaction; it is not shown in the plot. The exothermic reaction of sulfur with air (Eq. 8) releases more energy than the vaporization reaction of sulfur overlapping the endothermic curve. Ideally, a chemical reaction shows a single smooth peak in the DSC curves. However, in practice, other effects and reaction overlaps and distort the peak (like in peak 3).

$$S_8(s) + 8O_2(g) \rightarrow SO_2(g) \quad \text{(Eq. 8)}$$

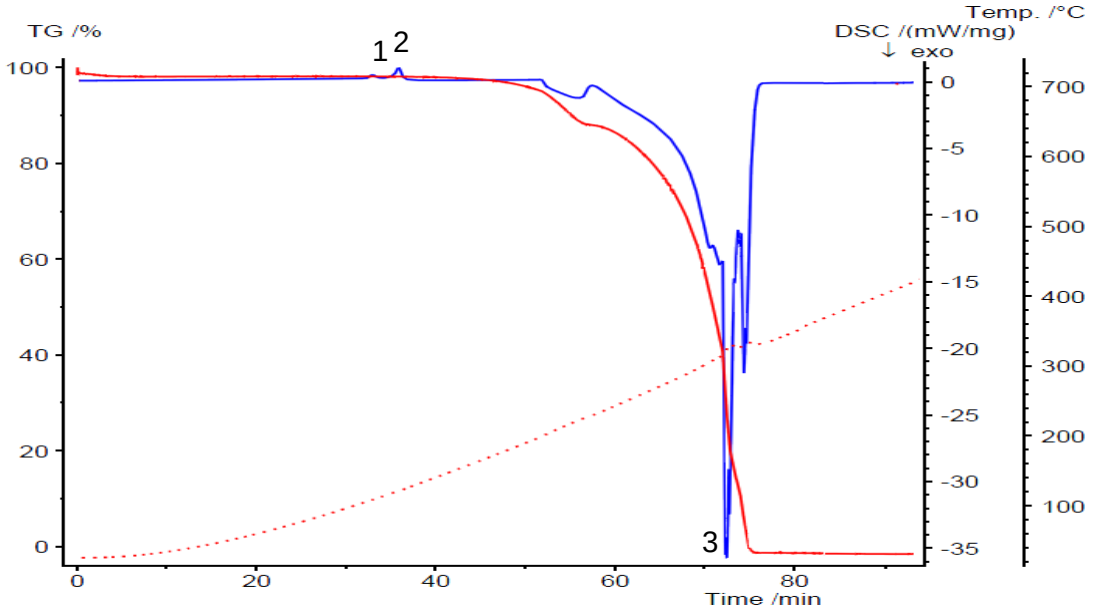

Figure 22: STA measurement of sulfur under air atmosphere. The red line is the mass loss and the blue line specific heat. The dashed line is the temperature.

In Figure 23, under argon atmosphere, it is possible to see that the DSC curve presents some differences when compared with the same curve of the Figure 22. Peaks 1 and 2, at 110°C and 122°C respectively, correspond as in Figure 22 to the sulfur melting point and they have almost the same values of temperature and enthalpy (see Table 5). So, once again, these two peaks correspond to α and β transition phases of the fusion of sulfur. Peak 3 at 300°C is associated with the vaporization phase of the sulfur because it occurs in the middle of the mass loss curve and the energy absorbed by the system is slightly higher than the melting energy. At the end, the energy curve keeps decreasing and it may correspond to the reaction of sulfur with air. Although all the precautions to avoid this from happening have been taken, air may have entered in the furnace leading to the formation of SO_2 and causing the asymmetry of the peak 3.

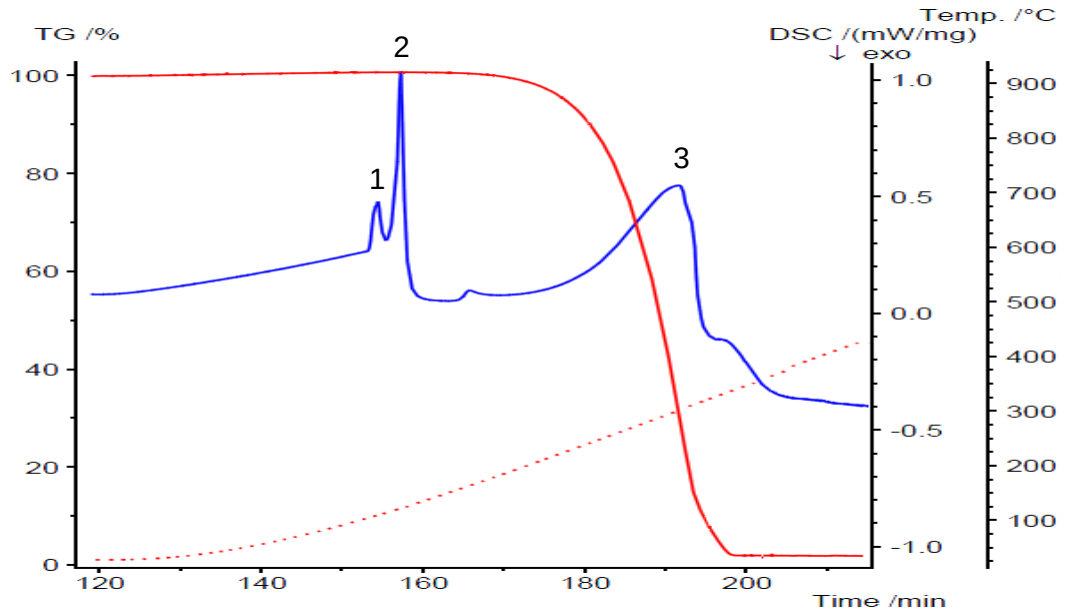

Figure 23: STA measurement of sulfur under argon atmosphere. The red line is the mass loss and the blue line specific heat. The dashed line is the temperature.

Table 5: Temperatures and enthalpies of sulfur measured under air and argon atmosphere. Exothermic process (negative sign) and endothermic process (positive sign).

Gas	Sulfur	Peak 1	Peak 2	Peak 3
Air	Middle Temperature (ºC)	109	122	325
	Enthalpy (J/g)	11	38	-7868
Argon	Middle Temperature (ºC)	110	122	300
	Enthalpy (J/g)	12	45	150

Figure 24 shows the results of the binder analysis. The DSC peak 1 at 156°C absorbs 2.4 J/g corresponds to the melting of PVDF (theoretical value near to 168°C). The material starts to decompose at 380°C. Peak 2 describes the combustion of PVDF with air at a middle temperature of 498°C and occurring simultaneously with the decrease of the TG curve. These combustion leads to formation of several products like H_2O, CO_2, CO and HF and is responsible for the high value of energy released.

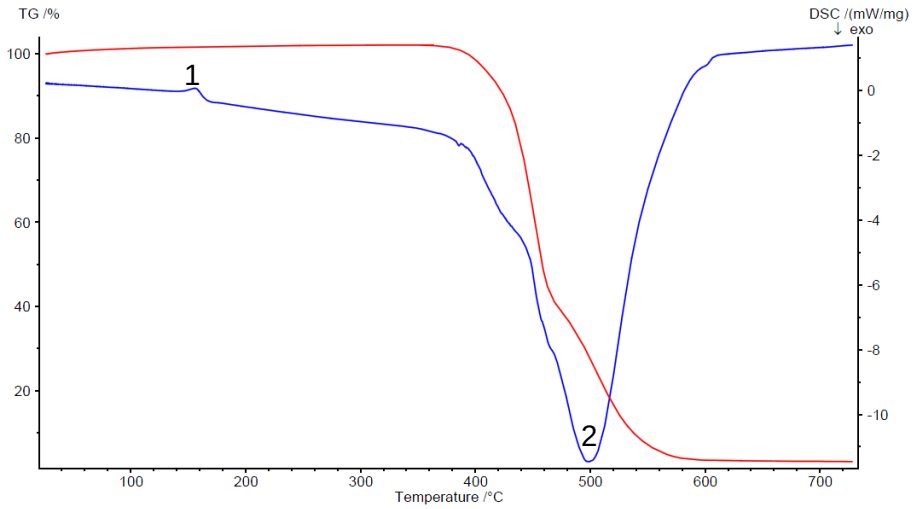

Figure 24: STA measurement of PVDF under air atmosphere. The red line is the mass loss and the blue line specific heat.

The analysis of carbon black is shown in Figure 25. In this measurement there is only one energy peak, it appears at 696°C matching with the decrease of the mass loss curve, and correspond to the reaction of CB with air (Eq. 9).

$$C(s) + O_2(g) \rightarrow CO_2(g) \quad \text{(Eq. 9)}$$

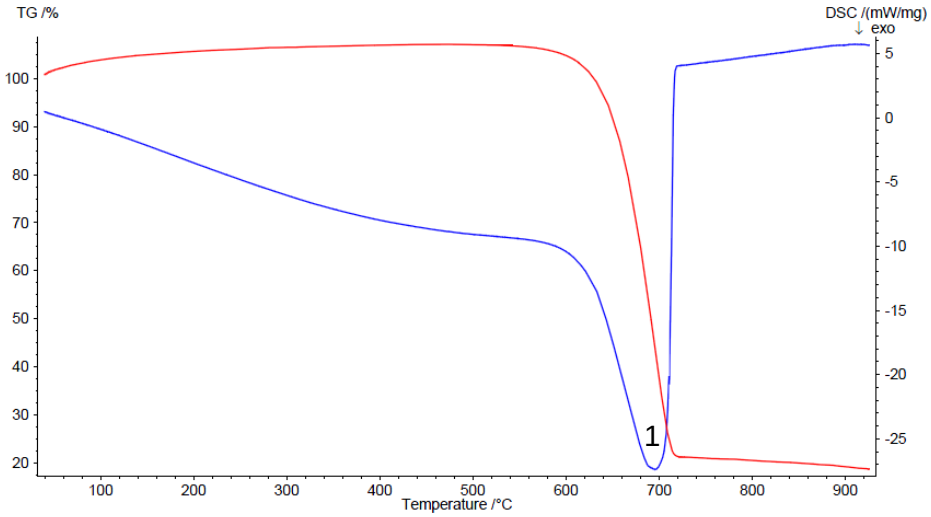

Figure 25: STA measurement of carbon black under air atmosphere. The red line is the mass loss and the blue line specific heat.

Table 6: Values of the temperatures and enthalpies of each peak of PVDF and CB measured in air atmosphere. Exothermic process (negative sign) and endothermic process (positive sign).

Gas	PVDF	Peak 1	Peak 2
Air	Temperature (°C)	156	498
	Enthalpy (J/g)	2	-11312
Gas	**Carbon Black**	**Peak 1**	
Air	Temperature (°C)	696	
	Enthalpy (J/g)	-14341	

4.2.2 Cathodes before cycling

Cathodes with 16 mm of diameter were tested with TG using the crucible shown in Figure 13b. Figure 26 shows a typical TG curve of one of the three cathodes before cycling displayed in the right corner. In Table 7, the mass loss averages and corresponding standard deviations are summarized.

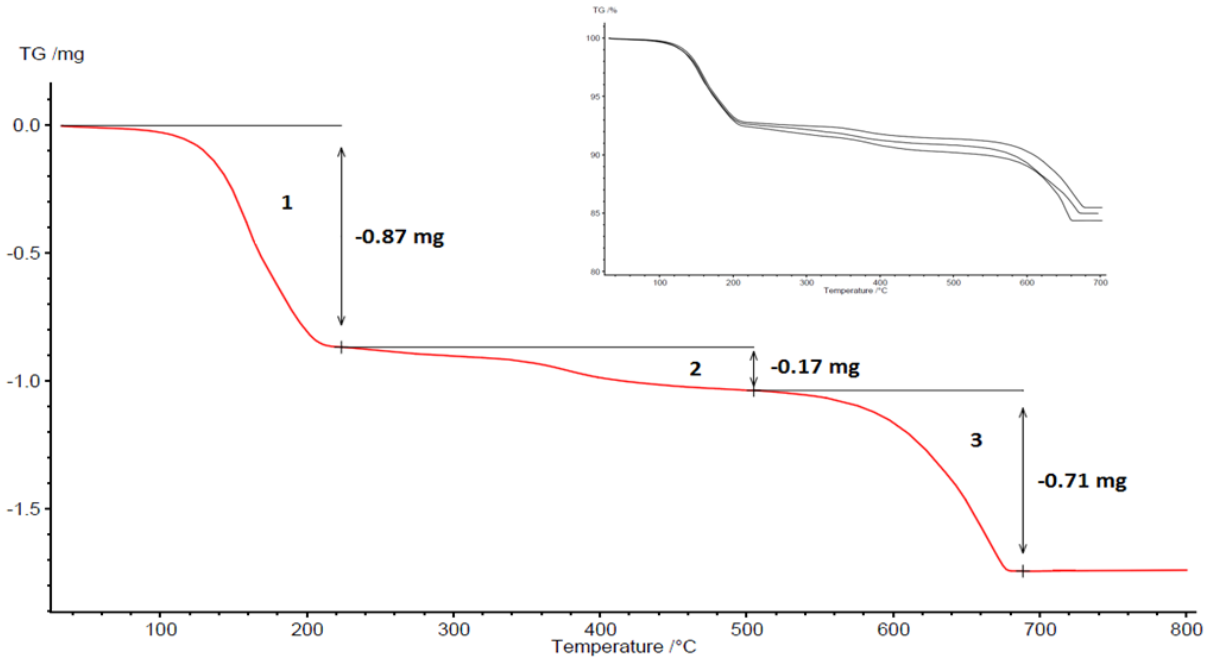

Figure 26: TG measurement of one cathode before cycling. On the right corner three TGA measurements of three cathodes.

The TG curve begins with a stable phase at the top. Then it has an abrupt mass loss (1) followed by a slight decrease at around 400°C (2). At higher temperatures (up to 500ºC) there is another decrease of mass (3). The temperatures at which these changes of masses occurs were compared with the previously values obtained for each component. Correlating the weight loss and the respective temperatures of the this figure with the ones of the individual components, it is possible to conclude that region 1 corresponds to the mass loss of sulfur, region 2 is the PVDF mass loss and the region 3 belongs to CB.

Table 7: TGA values of the three cathodes presented in Figure 26.

Cathode	Substrate + Layer (mg)	Layer (mg)	Sulfur (mg)	Sulfur (wt.%)	PVDF (mg)	PVDF (wt.%)	CB (mg)	CB (wt.%)
Average (3 samples)	12.20	1.83	**0.91**	**49.73**	0.21	**11.48**	0.71	**38.80**
Standard Deviation	0.29	0.07	0.03	0.45	0.04	1.66	0.02	1.57

In Table 7 there is the information about the weight percent of each component which is very similar with the ones of the initial cathode suspension reinforcing the previous conclusion. The PVDF region has the highest standard deviation for the relative weight which may

happen because this is the intermediate region and it could contain material coming from the others two regions at the same time.

An incorrect quantification of sulfur can conduct to errors in the specific capacity and density current. For this reason a pre-quantification of sulfur using TGA equipment should be done. In chapter 4.2.4 the results of one measurement using TGA to calculate the quantity of sulfur were compared to others where only the balance was used to weight the cathodes.

4.2.3 Cathodes after cycling

After analyze cathodes before cycling, cathodes after cycling were also tested with TGA and compared with the others. As can be seen in Figure 27, all the cathodes after cycling have the same main curves as the cathodes previously examined, but with some shifts. These variations happen at different temperatures and present different mass losses.

The mass loss of cathodes before cycling starts later, in other words, it starts for higher temperatures and, as can be seen, it happens for the sulfur and CB regions. The reason for this is the stronger binding of the particles before cycling, since the cathode material suffers important changes during the cycling. First, the cathode surface is covered with the electrolyte, immediately causing some changes. Then, during the cycling, the cathode surface is constantly changing because sulfur can diffuse in polysulfides which can pass through the separator, ultimately leaving the cathode. For these reasons, after cycling, the cathodes surfaces are not so stable, presenting a weaker binding which leads to loss of its mass at lower temperatures than the cathodes before cycling. Moreover, these reasons can also explain why the first main decreasing curves have a higher temperature range of the mass loss for cathodes before cycling.

The cathodes after cycling show a higher mass loss in the first curve. The cause is the presence of the rest of electrolyte salt products, which leaves the cathode at the same temperature as the sulfur, increasing the quantity of material lost.

For higher temperatures, the size of the second main curve (CB region) is similar for all the curves because at these temperatures there are only carbon black and substrate in all cathodes. In this case, mass loss is similar. However, the curves after cycling appear 200ºC before, confirming their lower stability when compared with the ones of the cathodes before cycling.

Among the cathodes after cycling, it is difficult to find a logical sequence between their mass loss and the number of cycles. Although one could expect to find more quantity of sulfur for low number of cycles, Figure 27 shows that does not happen. The explanation for this can be related with the moment of disassembling the battery, more specifically, when the separator is removed out of the cathode. During the disassembling the quantity of cathode

material is randomly distributed and sometimes a few quantities remain in the separator leading to a loss of sulfur.

For cathodes after cycling the PVDF region is not detected, the cause for this may be a possible degradation of the polymer during cycling.

A cathode without cycling was dried with a small volume of electrolyte in order to see if the electrolyte was causing the shifting of the curves. The result is displayed by the yellow curve. It has the longest first curve. Despite the fact that the quantity of electrolyte has been the same for all cathodes after cycling and also for this one, in this case the cathode was immediately dried in the oven for some days with electrolyte over its surface. This may have caused a higher aggregation of the particles leading to a higher resistance against the increase of temperature. However, the starting temperature of carbon black mass loss is the same as the other cathodes before cycling because, once again, at these higher temperatures the cathode has only CB and the substrate.

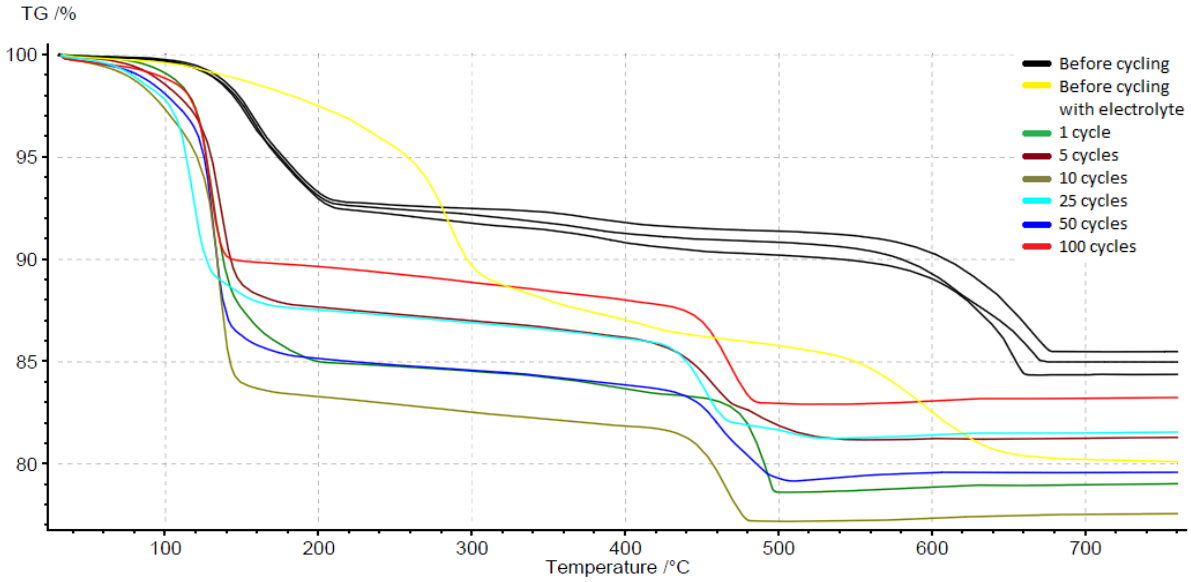

Figure 27: Mass loss of cathodes before and after several cycles against temperature

In Figure 28 it is possible to see the same TG measurements coupled with MS. The compound analyzed in MS is the reaction product of the oxidation of sulfur under air: SO_2. Once more, it is not possible to create a logical sequence for the mass loss among the cycled cathodes even with the support of the MS results. However, it can be seen that the peaks of SO_2 corresponding to the cathodes after cycling appear at the same temperature as the first TG decreasing curve, confirming the presence of sulfur at this moment of the measurement.

The peak of SO_2 of the cathode before cycling has a peak area larger than the others due to its higher quantity of sulfur, since this cathode did not have any change in its surface. However, there is a strange delay comparing with the curve of sulfur mass loss. In order to

understand this delay, several TG/MS measurements were made for cathodes before cycling, obtaining similar results. A possible explanation may be a first evaporation of sulfur and an oxidation at higher temperature. In the case of the cathode after cycling, smaller particles may be present, making easier the oxidation reaction and leading to an almost instantaneous appearance of the ion current peak during the weight loss.

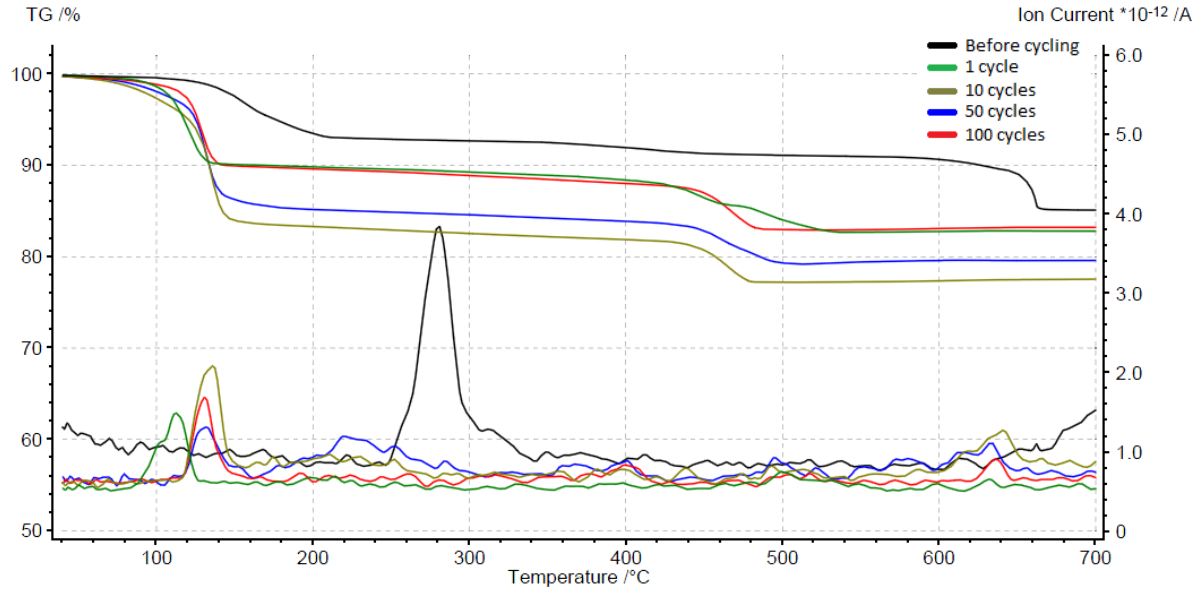

Figure 28: TG measurements coupled with SO_2 detected in MS measurement.

Figure 29 illustrates the same measurements presented before, plus the STA and MS tests of the elemental sulfur, with the purpose of comparing its behavior with the cathode's one. The quantity analyzed was similar with the one that is usually present in these cathodes (approximately 0.6 mg).

In Figure 29, the ion current curve of the elemental sulfur has the highest peak and it is related to the quantity of sulfur present in the measurement. This peak appears immediately after the mass loss curve and, when compared to the cathodes. Whereas in the cycled cathodes these peaks happens at the same time as the mass loss curve, and in the cathode before cycling it happens much later, in the elemental sulfur case it appears right in the end of the mass loss curve. The reason of this may be a first evaporation of sulfur and then an oxidation at higher temperature.

The size of the particles as well as the binding may have an important role in the evaporation and oxidation processes. The elemental sulfur particles are larger but not bonded with PVDF, this explain the lower start temperature of mass loss in comparison with the sample before cycling. As explained before, the particles of the cathodes after cycling may smaller and may be aggregated on the cathode surface. In Figure 29, it is possible to verify that these particles react even more easily with O_2.

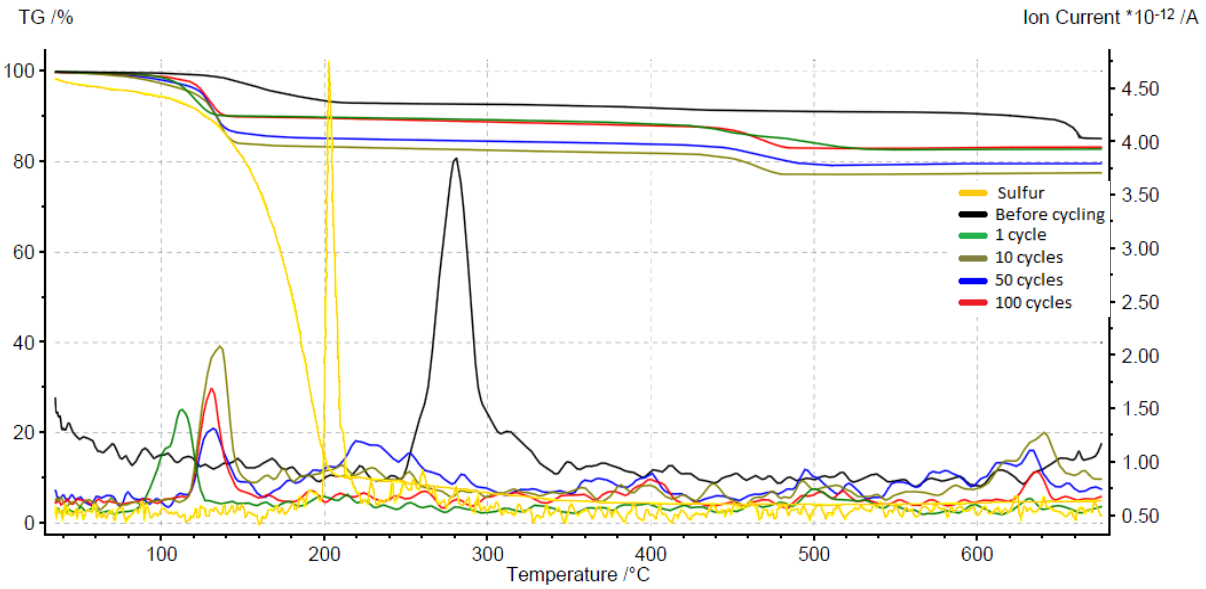

Figure 29: TG measurements coupled with SO_2 detected in MS measurement.

Figure 30 shows the results for the mass number 44: CO_2. All the ion current curves appear at the same time as the second main mass decreasing curve. It confirms the combustion of the CB at these temperatures (approximately 450°C for cycled cathodes and 650°C for cathodes before cycling) and the higher stability of the cathodes before cycling. At the beginning, there are small peaks occurring at the same time as the loss of the sulfur which may be related with the reaction of some components of the electrolyte with air.

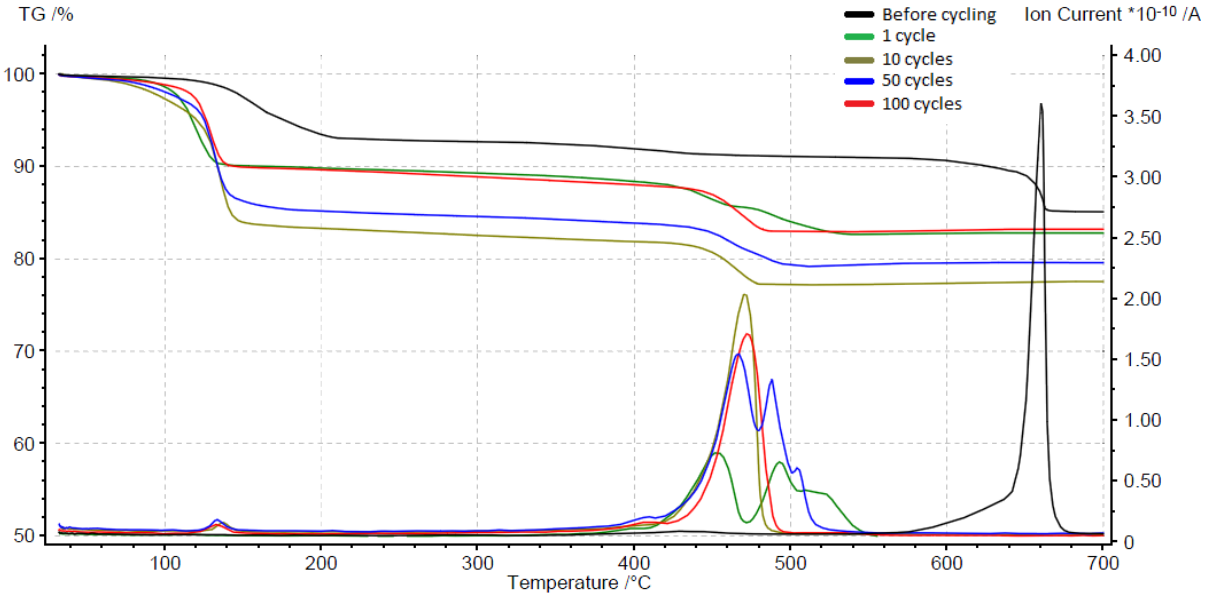

Figure 30: TG measurements coupled with CO_2 detected in MS measurement.

More compounds were detected during these measurements and some of them are displayed in Annex D.

4.2.4 Importance of TGA measurements

During this experimental work some batteries using 16 mm diameter cathodes presented higher discharge capacity than the maximum theoretical value (1675 Ah/kg). A study was made in order to find the error of these measurements. Table 8 shows the mass values obtained from the balance of one of these batteries. The substrate weight is an average of three measurements.

Table 8: Weight of the components of the one 16 mm diameter cathode.

Cathode	Weight (mg)
Layer + Substrate	12.13
Substrate	11.05 ± 0.3
Layer	1.08
Sulfur	0.54

In Figure 31 it is possible to see the curve (black) of the discharge capacity of this battery obtained from the BaSyTec equipment after introduce in its system 0.54 mg of sulfur weighted from the balance. The initial values are higher than the theoretical discharge capacity value which means that some error occurred.

After multiplying the discharge capacity values (Ah/kg) by the weight of sulfur ($0.54x10^{-6}$ kg), the values of the electric charge (Ah) are obtained. The division of the electric charge values by the average value of the sulfur taken from the Table 7 (0.91 mg) makes possible the calculation of new discharge values (Figure 31 red line). These new curve presents values very similar with the ones of the average of the small batteries, confirming the error of the first measurement and reinforcing the theory of the higher precision of the values coming from the TGA.

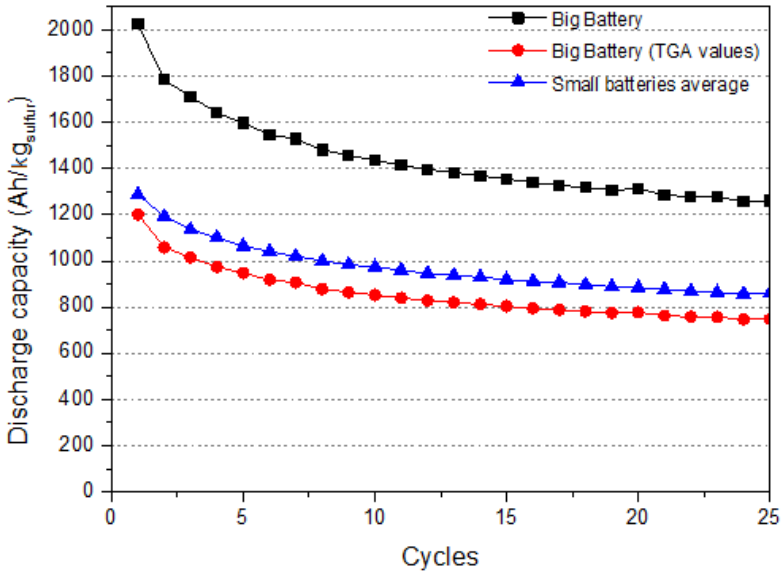

Figure 31: Discharge capacity of big and small batteries.

4.2.5 Quantification and distribution of sulfur particles after cycling

In order to quantify the sulfur transferred from the cathode to the separator during the battery operation, these two components were analyzed by means of mass spectrometer. Two batteries with different number of cycles were chosen (Battery A – 10 cycles; Battery B – 100 cycles). Figure 32 illustrates the results for the mass number 64: SO_2 .The ion current peaks appear in a similar range of temperature but their sizes are different. The separators peaks have a larger area than the ones of the cathodes meaning that the separators hold more quantity of sulfur in their surface.

The peak area of the evolved gas SO_2 from the mass spectrometer can be correlated linearly with the mass loss of sulfur measured by TGA for cathode before cycling. Using the areas of Figure 32, the quantity of sulfur was estimated in these batteries (Table 9).

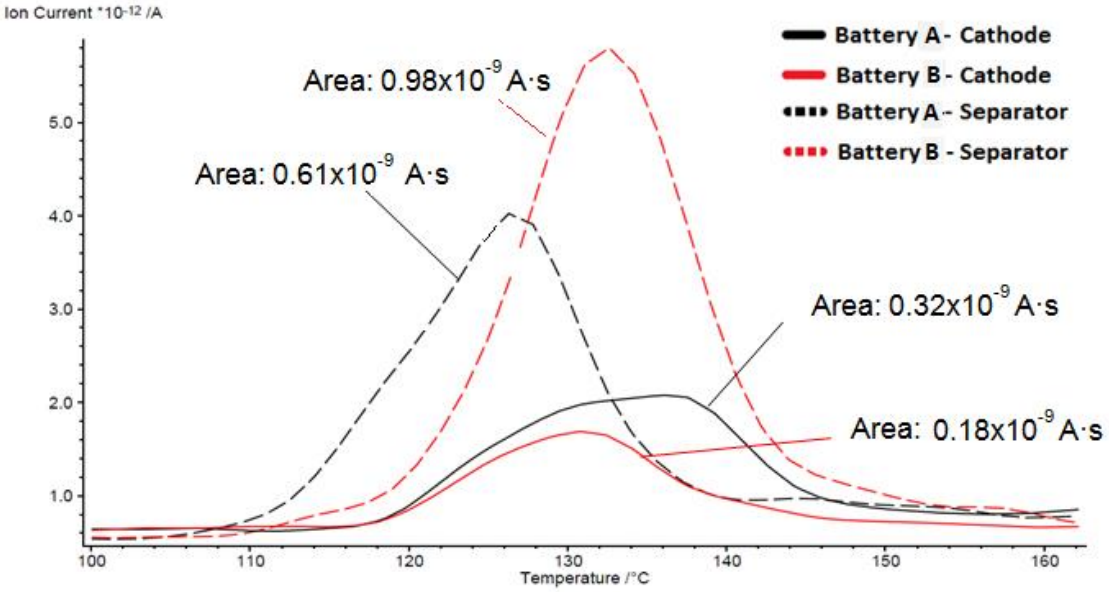

Figure 32: Ion current peaks of SO2 of the components of the battery 1 and battery 2.

The results show that battery A has lower quantity of sulfur (0.73 mg) comparing with the value of the average obtained in TGA for cathodes before cycling (0.91 mg) Table 7. The values of the battery B indicates that after 100 cycles, the sum of the weights of the sulfur is exactly the same of the average obtained by TGA (0.91 mg). It may mean that the polysulfides formed during the battery operation remain in the battery after dried its components, contributing for the maintenance of the sulfur weight. These two batteries were also analyzed by means of TGA (additional information) but the TG curve of the separators is unstable due to their light weight and large size (22 mm - overcome the crucible borders)(TG curve can be seen in Annex D). It is possible to say that mass spectroscopy can be used to quantity the amount of sulfur present in the battery, however some

improvements have to be done in order to stabilize the TG curve of separators obtaining that way more reliable results.

Table 9: Areas and weight corresponding to the peaks of the Figure 32.

Mass Spectroscopy	Cathode BF	Battery A			Battery B		
		Cathode	Separator	Total	Cathode	Separator	Total
Area (nA·s)	1.08	0.32	0.61	0.93	0.18	0.98	1.16
Weight$_{Sulfur}$ (mg)	0.85	0.25	0.48	**0.73**	0.14	0.77	**0.91**

4.3 Influence of intermediate layers

A micro-porous carbon diffusion layer (CDL) and a nano-porous carbon black layer (SC: +CB) were tested and compared with the simple cathode (SC). Both layers were added in order to lodge the sulfur particles during the cycling, avoiding their passage through the separator. The results of the cycling tests are presented in Figure 33.

In Figure 33 a) the batteries SC:CDL and SC:+CB present the highest initial discharge curves. The initial value of the CDL is very close to the theoretical capacity (1675 Ah/kg) and the one of the +CB is even higher than this theoretical value. This high value can be associated with an error of the sulfur mass calculation for these batteries. All the batteries suffer gradual capacity degradation. At the 100th cycle the batteries with the simple cathode (SC) present the highest discharge curve near 500 Ah/kg.

Figure 33 b) shows that all the batteries have coulombic efficiency values near 100 %, which means that the discharge and charge values are almost identical. This is attributed to the electrolyte E_4. The SC presents a slightly more stable efficiency than the others.

Both intermediate layers only improve the batteries performance in the initial cycles, suffering higher degradation during the cycling when compared with SC.

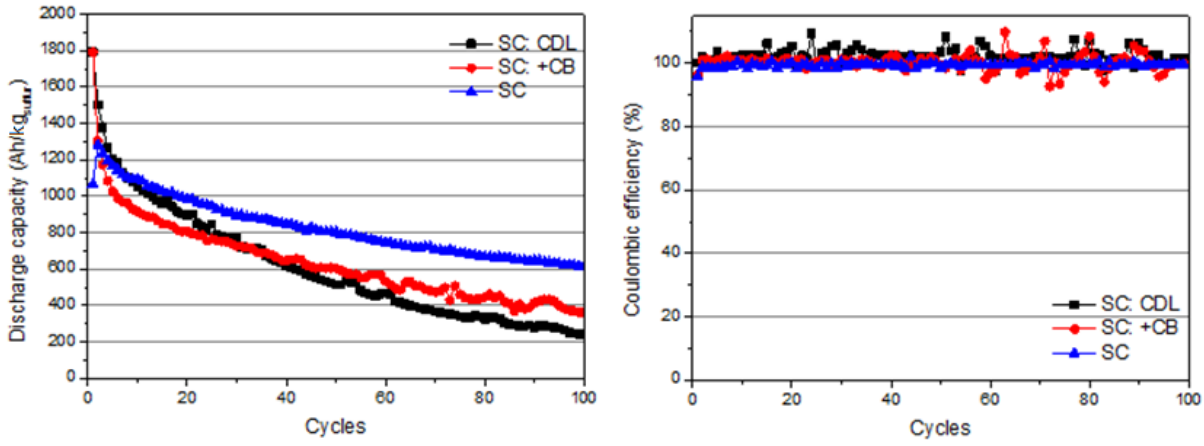

Figure 33: a) Discharge capacities curves for SC, SC:+CB and SC:CDL b) Charge-discharge efficiency for the respective batteries.

Microscopic pictures were taken over the surfaces of these two layers and also over the respective separators to see if the formation of sulfur over the separator was avoided.

Figure 34 corresponds to SC:CDL components after 100 cycles. Image a) presents a homogenous cathode's surface, where is not possible to see sulfur with the microscopic resolution, as well as the picture of the CDL. On the other hand, separator surface reveals a high quantity of sulfur.

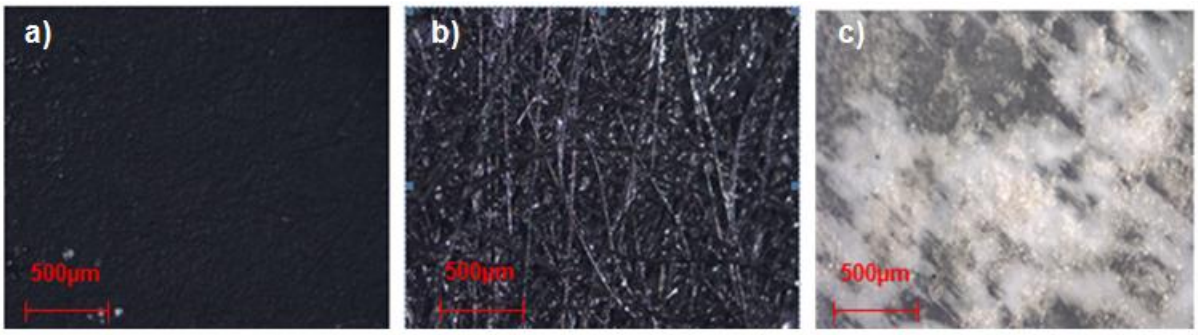

Figure 34: a) SC: CDL- cathode; b) CDL layer; c) separator (anode side).

In order to obtain a higher magnification of these samples, SEM pictures were taken over the CDL. These pictures can be seen in Figure 35. In these pictures, sulfur is not identified and is not lodged on the porous of this layer which confirms the microscopic results. The reason for these is related to the porosity of the CDL which is probably too high to retain the sulfur particles leading to their appearance on the other side of the separator.

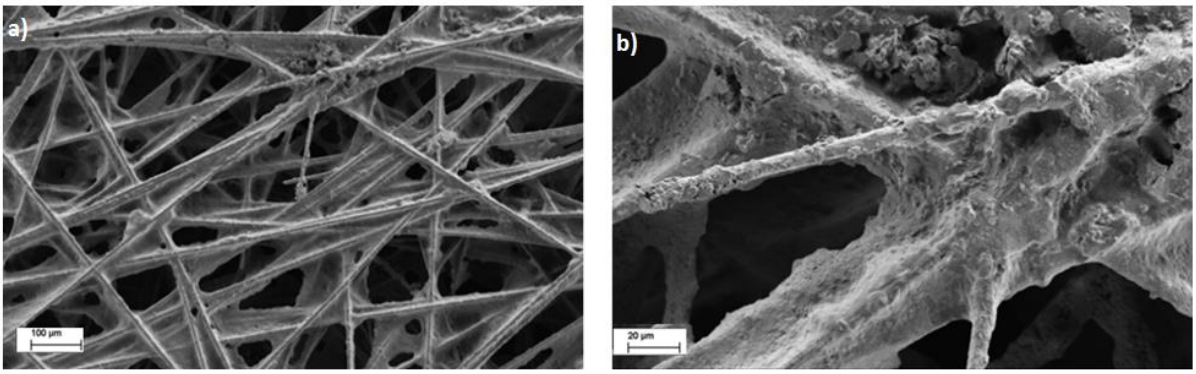

Figure 35: SEM images of CDL. Magnification: 100x (a) and 500x (b).

Figure 36 illustrates the microscopic pictures of the cathode and separator of a battery with the extra CB layer (SC: +CB) after 100 cycles. The cathode surface is homogeneous after 100 cycles showing only the CB layer without any sulfur; however the separator presents high quantity and large agglomerates of sulfur crystals. The additional nano-porous layer did not avoid the passage of the sulfur particles to the other side of the separator, explaining the loss of capacity during cycling.

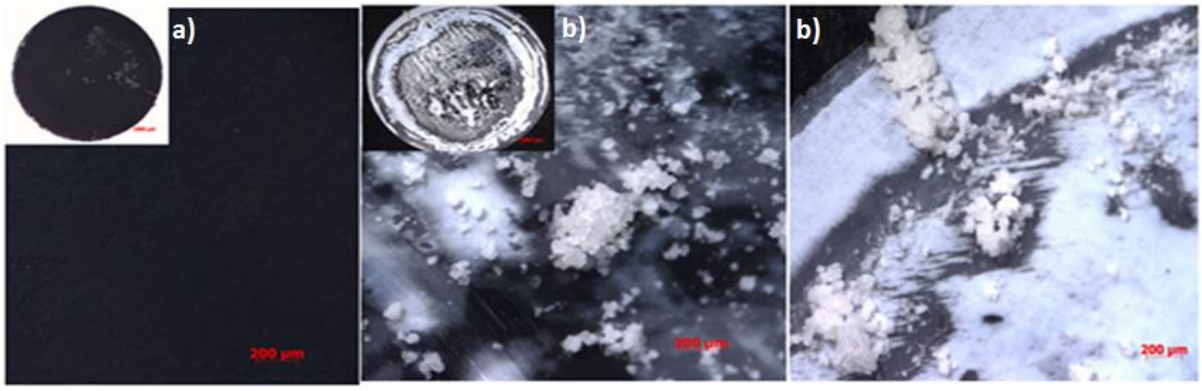

Figure 36: a) Cathode and b) separator (anode side) of the battery SC:+CB after 100 cycles.

The SEM pictures taken over this cathode before and after cycling are presented in Figure 37. In the cathode before cycling, sulfur is almost completely covered by the CB layer. However, after 100 cycles some cracks are shown on its surface (Figure 37 c), which might be caused by the outflow of the sulfur particles. Figures 37 d) presents sulfur spread over the surface of the cathode which means that not all sulfur had left the cathode during the operation of the battery. Nevertheless, low retention of sulfur was achieved since high quantity of sulfur had been found on the other side of the separator.

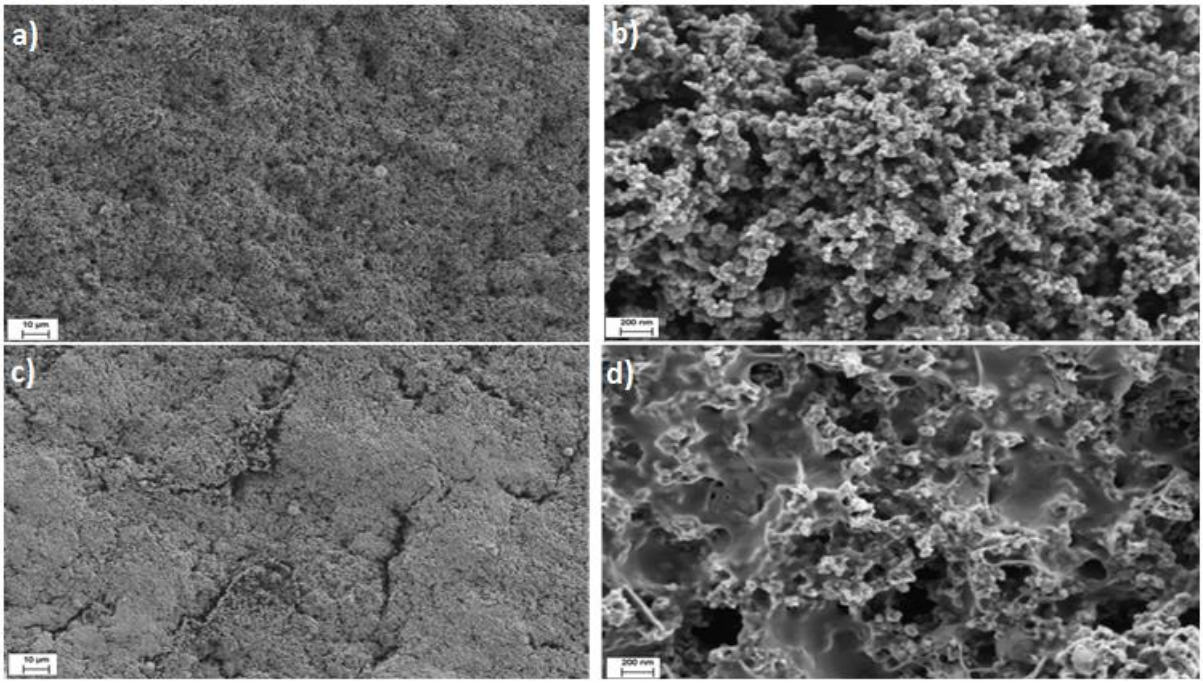

Figure 37: SEM pictures of the SC:+CB battery: a,b) before cycling; c,d) after 100 cycles. Magnification: 300x (a-c) and 30000x (b-d).

5. Conclusions

The application of TGA, DSC and EGA for cathodes analysis of Li-S batteries was successfully tested.

- STA is a useful technique to evaluate the behavior of the battery components separately, namely their variation of weight and energy during the increase of the temperature. The change of the gas atmosphere can be used to avoid undesired reactions between these components and air.
- With TGA equipment it was possible to determine the exact composition of the cathode before cycling (important for an accurate calculation of the specific capacity).The exact quantification of sulfur after cycling was not possible with TGA due to the presence of electrolyte components.
- Coupling TGA to EGA was an advantageous method to go deeper in this investigation, namely during the identification of the different gases released. The analysis to SO_2 showed that only the TG curves of the cathodes after cycling match with ones of ion current. With mass spectroscopic testes is possible to calculate the mass of sulfur present in the cathode and separator, with a previous linear correlation of mass loss of sulfur (TGA) and peak area of SO_2 (MS).
- The stability of cathode can be evaluated with these techniques (weaker binding of conductive particles and degradation of the binder). Cathodes after cycling are clearly more unstable than the ones before cycling.

It was possible to investigate the cycling stability and morphological changes of Li-S batteries:

- The battery performance is improved by the addition of $LiNO_3$ into the electrolyte, presenting higher values of discharge capacity and higher coulombic efficiency (around 100% during 100 cycles) which avoided the shuttle mechanism due to formation of a protective film over the anode. Sulfur can be detected in the cathode after 100 cycles, and also over the separator.
- The separators using E4 as electrolyte present more quantity of sulfur in their surfaces than the ones using E0. For higher number of cycles the cathode shows lower quantity of sulfur, but high accumulation of sulfur occurs over the separator
- For high C-rate the discharge capacity is relatively constant but it is also low, never reaching 600 Ah/kg after 85 cycles. For low C-rate the initial discharge capacity is the highest, however it also presents the highest degradation.

The intermediate layers did not influence positively the batteries performance. Sulfur particles were no retained in neither on microporous or nano-porous layers over the cathode, therefore no capacity improvements were achieved

5.1 Limitations and future work

The single utilization of TGA was not enough to quantify the amount of sulfur in cathodes after cycling due to the presence of the electrolyte salt products. For this reason TGA was coupled with MS and more information was obtained. However, the total weight of sulfur could not be estimate because part of this weight was stuck in the separator. Then measurements of the separators were also done. The sum of the ion current peaks of SO_2 coming from the separators and the cathodes showed valid results. Nerveless, these results were not precise due to instability of the separator TG curve caused by the light weight and large size of the separator. In a future work the TGA/MS analysis of cathode and separator as a single sample could be a good option to avoid the loss of the sample material. However, this procedure would restrict the study of the internal surfaces of these components. Another way to hold the sample like a closed crucible or a larger diameter could be a valid option. Small cathodes (10 mm diameter) and big cathodes (16 mm) but with lower quantity of sulfur, were also investigated in MS analysis. However, this equipment was not able to detect the presence of sulfur. For future measurements only cathodes weighing more than 12 mg should be measured.

The intermediate layers did not retain the sulfur particles. However, the nano-porous layer (SC: +CB) showed some sulfur on its surface after 100 cycles, may be testing this same layer with higher thickness would improve the retention of sulfur.

6. References

[1] P. Arora, Z.J. Zhang, Chemical Reviews 104 (2004) 4419.

[2] http://www.science.uwaterloo.ca/~lfnazar/research.htm#top, NazarGroup, (2013).

[3] M.-K. Song, E.J. Cairns, Y. Zhang, Nanoscale (2013).

[4] S.S. Zhang, Journal of Power Sources 231 (2013) 153.

[5] Z. Deng, Z. Zhang, Y. Lai, J. Liu, J. Li, Y. Liu, Journal of the Electrochemical Society 160 (2013) A553.

[6] V.S. Kolosnitsyn, E.V. Karaseva, Russ. J. of Electrochem. 44 (2008) 506–509.

[7] Y. V. Mikhaylik, J.R. Akridge, Journal of The Electrochemical Society 151 (2004) A1969.

[8] X. Ji, K.T. Lee, L.F. Nazar, Nature Materials 8 (2009) 500.

[9] Y. Yang, G. Zheng, Y. Cui, Chemical Society Reviews (2013).

[10] B. Ding, C. Yuan, L. Shen, G. Xu, P. Nie, Q. Lai, X. Zhang, Journal of Materials Chemistry A 1 (2013) 1096.

[11] S.S. Zhang, Journal of Power Sources 231 (2013) 153.

[12] Y. Huang, J. Sun, W. Wang, Y. Wang, Z. Yu, H. Zhang, A. Wang, K. Yuan, Journal of The Electrochemical Society 155 (2008) A764.

[13] L.D.J.Y.C. S. J. Visco, E. Nimon, B. Katz, Lithium/sulfur batteries with high specific energy: old challenges and new opportunities, Nanosclale 2013

[14] D. Marmorstein, T.H. Yu, K.A. Striebel, F.R. Mclarnon, J. Hou, E.J. Cairns, (2000) 219.

[15] W. Wang, Y. Wang, Y. Huang, C. Huang, Z. Yu, H. Zhang, A. Wang, K. Yuan, Journal of Applied Electrochemistry 40 (2009) 321.

[16] X. Liang, Z. Wen, Y. Liu, M. Wu, J. Jin, H. Zhang, X. Wu, Journal of Power Sources 196 (2011) 9839.

[17] J.-W. Choi, G. Cheruvally, D.-S. Kim, J.-H. Ahn, K.-W. Kim, H.-J. Ahn, Journal of Power Sources 183 (2008) 441.

[18] U. of W. Susan Swapp, Geochemical Instrumentation and Analysis, SEM (2013).

[19] http://serc.carleton.edu/research_education/geochemsheets/techniques/XRD.html, 67 (1995) 271A.

[20] http://content.piacton.com/Uploads/Princeton/Documents/Library/UpdatedLibrary/Raman _Spectroscopy_Basics.pdf.

[21] D.A.E. Ashcroft, M.S.F. Manager, A.C. for S.M. Biology, A. Building, T.U. of Leeds., (2013).

[22] http://wiki.answers.com/Q/What_is_UV_spectroscopy, Date Accessed: 25.04.13.

[23] M.I.T. Electric, V. Team, A Guide to Understanding Battery Specifications (2008).

Additional Information

Appendix A

Influence of the $LiNO_3$ as additive

Figure 38 illustrates the average of the discharge capacity of 9 batteries using E4 and 4 four batteries using E0 after 25 cycles.

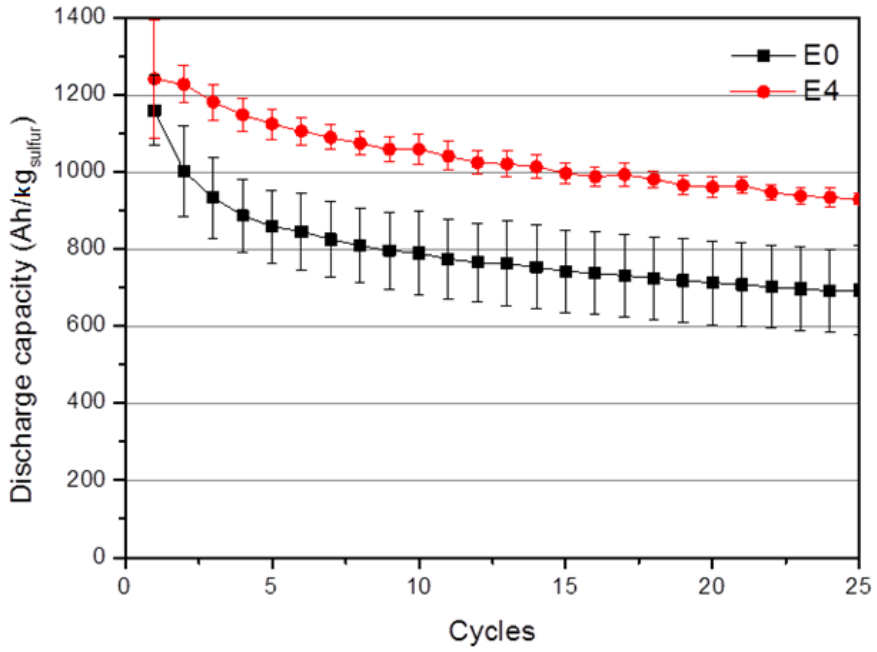

Figure 38: Discharge capacity curves for batteries tested with E0 and E4 as electrolyte

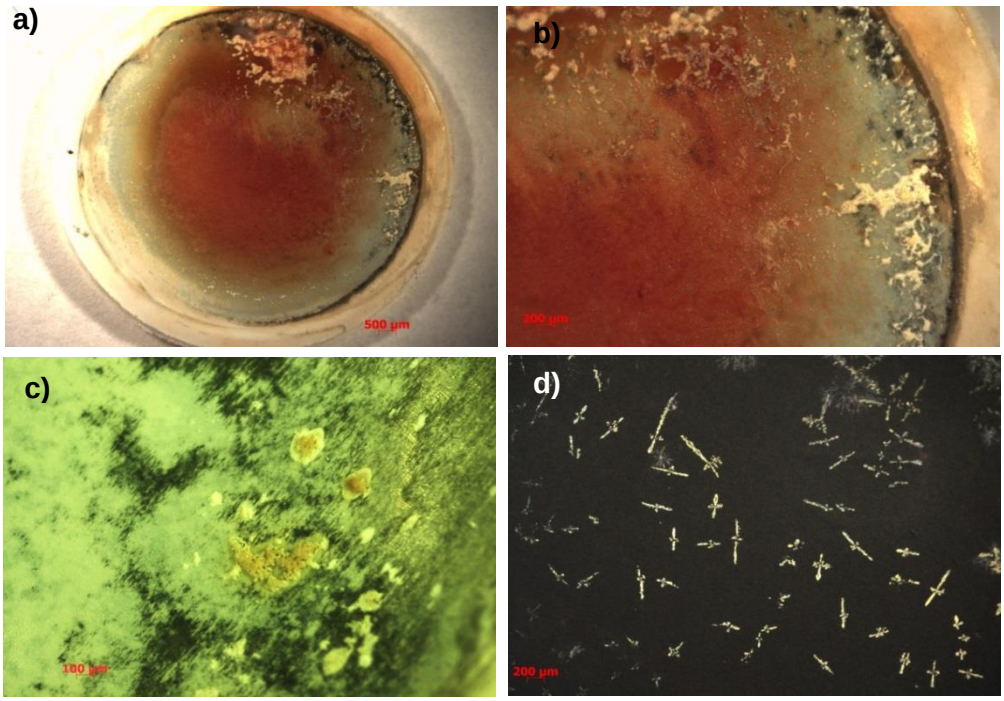

Figure 39: a) and b) after 64 cycles separator using E0; c) separator after 25 cycles using E4; d) cathode after 11 cycles using E0.

Appendix B

DSC Analysis

Table 10: Thermal data for phase transition of sulfur

Transition	Process or reaction	T, K	ΔH, kcal/g-atom[a]	ΔS, cal/deg·g-atom	Ref
α, β	α-S_8(s) → β-S_8(s)	368.46 ± 0.1	0.096	0.261	119, 128
Sublimation α	α-S_8(s) → cyclo-S_8(g)	368.5	2.979	8.191	
β	β-S_8(s) → cyclo-S_8(g)	368.5	2.883	7.93	172
ϵ	ϵ-S_6(s) → cyclo-S_6(g)	300	4.02	8.38	6
Fusion α	α-S_8(s) → cyclo-S_8(l) + ?[b]	383[c]	0.507		52, 119, 122, 172
β	β-S_8(s) → cyclo-S_8(l) + ?[b]	392.9[c]	0.3842	0.75	173, 174
λ, π	cyclo-S_8(l) → catena-S_8(l)	432	4.1	2.88	71, 193
Polymerization	catena-S_8(l) + cyclo-S_8(l) → catena-S_8(l)	442.8	0.396[d]	0.58	10
Vaporization	S_l(l) → S_l(g)	717.824[e] = 444.674 °C	2.5	3.5	6

[a] 1 g-atom of sulfur = 32.066 g. [b] The composition of the melt is not known. [c] See also Table XIV. [d] See ref 10. [e] Sulfur is a secondary temperature reference point on the International Practical Temperature Scale, ref 201.

STA

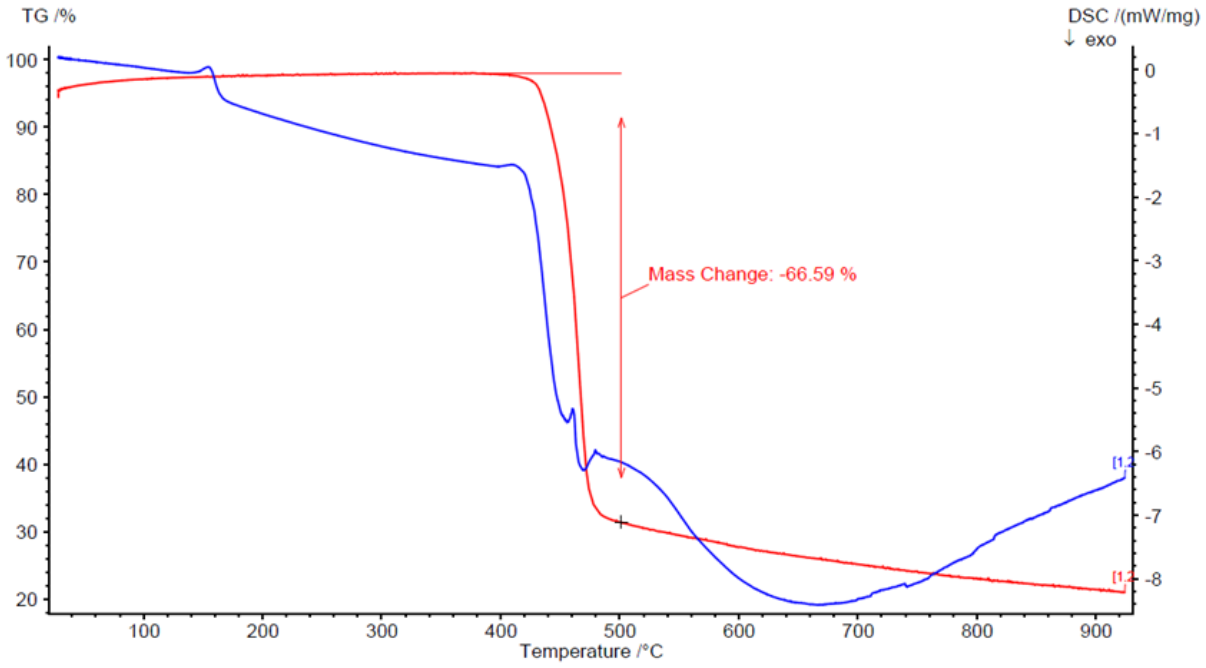

Figure 40: STA measurement of PVDF under argon atmosphere. The red line is the mass loss and the blue line specific heat. The dashed line is the temperature.

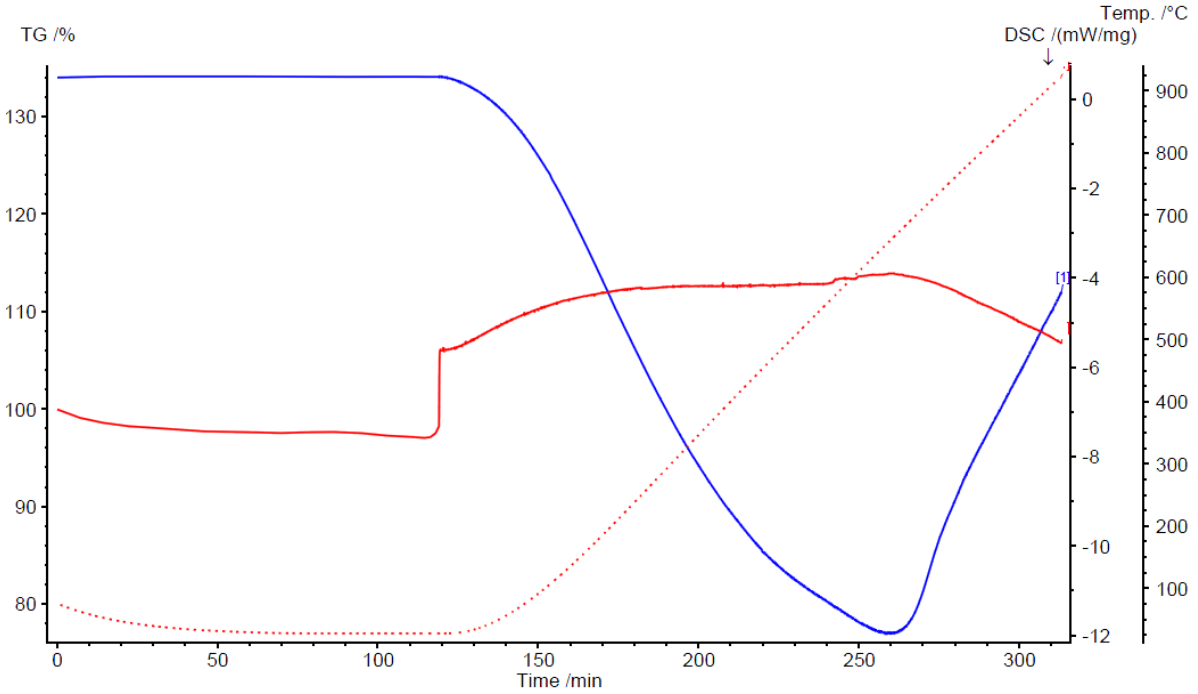

Figure 41: STA measurement of CB under argon atmosphere. The red line is the mass loss and the blue line specific heat. The dashed line is the temperature.

Appendix C

SEM images

In order to identify the different regions observed in SEM pictures of the cathode´s surface, EDX analysis were used. Figure 41 shows a cathode after cycling where four regions of its surface were analyzed.

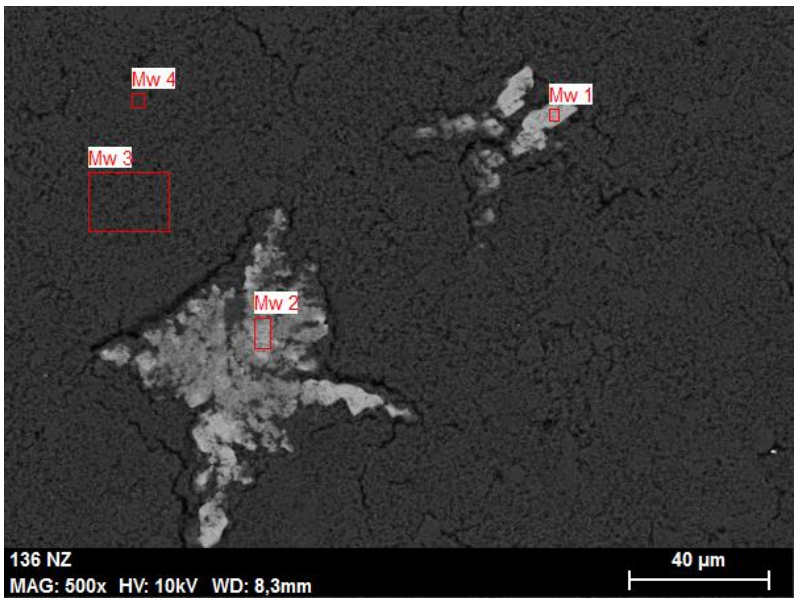

Figure 42: SEM image of one cathode after 100 cycles.

Figure 43 presents the EDX analysis identifying the components contained by the regions selected. The results show the presence of sulfur in all regions with higher quantity for the

first two. Fluor is also detected probably coming from the electrolyte salt products. As expected, carbon peaks appear belonging to carbon black. Is important to highlight that after 100 cycles, the highest quantity of sulfur is on the surface, it happens because sulfur is the end product of the reactions occurring during the Li-S battery operation.

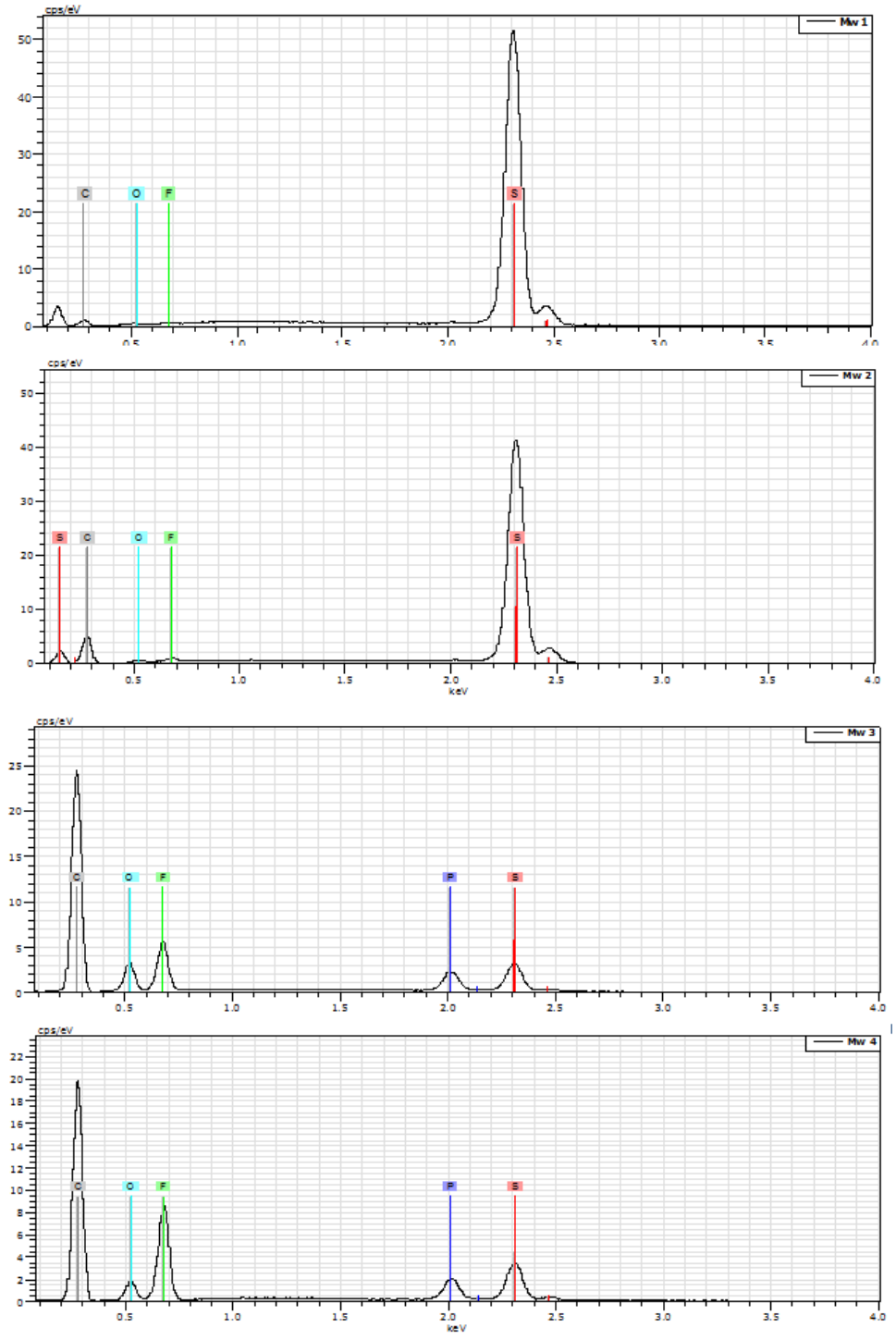

Figure 43: EDX analysis of the Figure 41.

Appendix D

Mass spectroscopy

In chapter of the results and discussion, SO_2 and CO_2 were the only gases analyzed by the mass spectrometer. However other gases were detected during these analyses. Figure 44 illustrates the main variations of gases by their molecular mass during the analysis of one cathode before cycling. The molecular masses (48, 50, 64, and 66) belong to sulfur oxides like SO_2 and SO (Figure 45 and 46 can help in this identification). CO_2 is detected by the molecular masses number 12, 44 and 45. H_2O corresponds to number 18 and the number 19 indicates the presence of fluor coming from the binder.

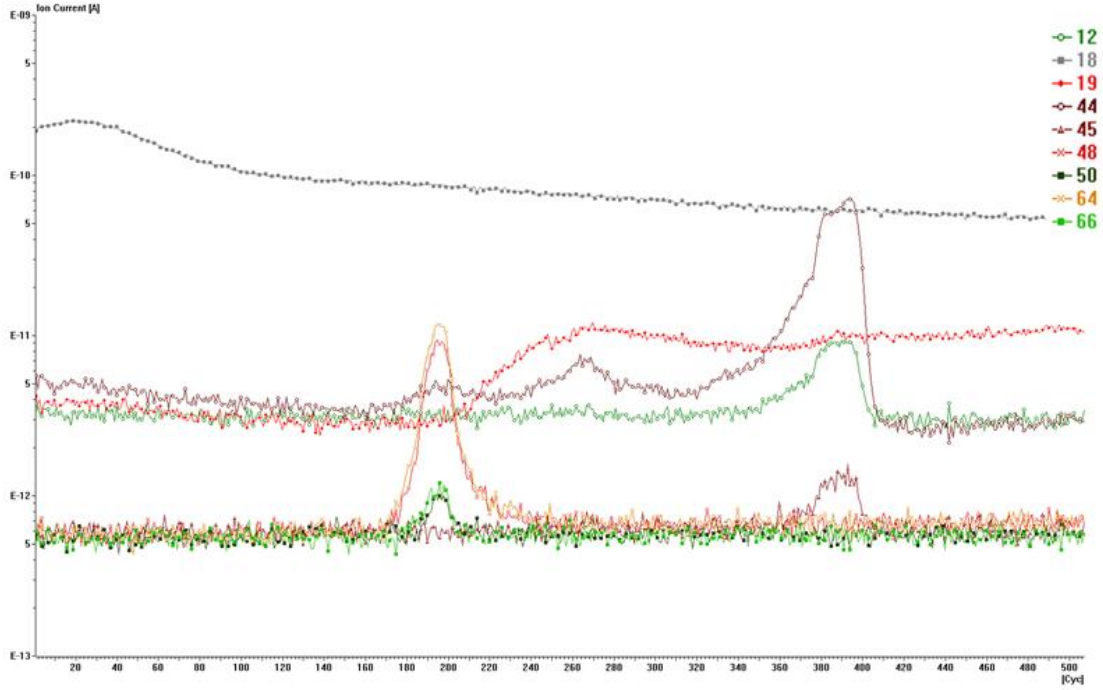

Figure 44: Mass spectrometer results of one cathode before cycling

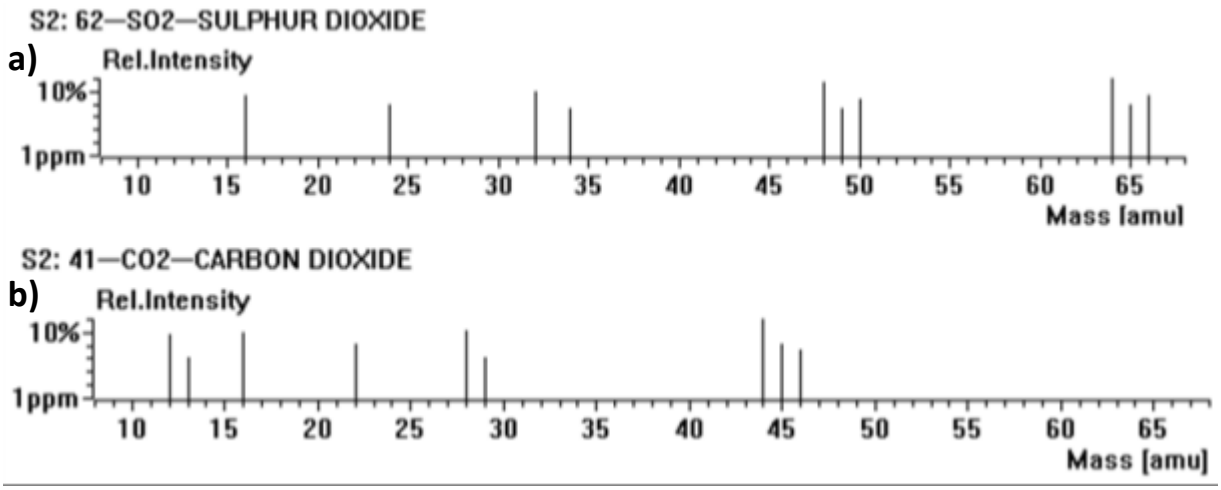

Figure 45: Mass spectrum: a) SO_2; b) CO_2

Massenzahl	H_2	He	CH_4	H_2O	Ne	N_2	CO	C_2H_6	O_2	Ar	CO_2	C_3H_8
1	3		16,5	2,4				9,6				5,0
2	100											
4		100										
12			3,0				6,3	0,7			9,7	0,6
13			7,8					1,2				0,9
14			16,0			14	0,8	3,3				2,3
15			85,0					4,7				7,2
16			100	1,8			2,8		18		16,0	
17			1,2	26								
18				100								
20					100					22,6		
22					10,2						2,1	
25								3,8				0,8
26								22,2				9,8
27								33,4				43,5
28						100	100	100			13,0	61,0
29						0,7	1,2	20,0				100
30								22,2				21,7
31												
32									100			
34									0,4			
36										0,34		
37												4,6
38										0,06		6,7
39												20,2
40										100		2,6
41												15,0
42												4,8
43												22,8
44											100	24,0
45											1,2	0,8

Figure 46: Relative ion current of ion fragments (Massen zahl = mass number)

In order to quantify the sulfur present on the separator surface after cycling, TGA/MS measurements were also made. Figure 47 illustrates the TG and ion current curves (SO_2) of two cathodes after 10 and 100 cycles. The TG curves are unstable due to light weight of the separator and because of its bigger diameter which overcome the borders of the crucible. In spite of this problems related with weight of the sample, it ion current peaks indicate the presence of SO_2 during the loss of sulfur.

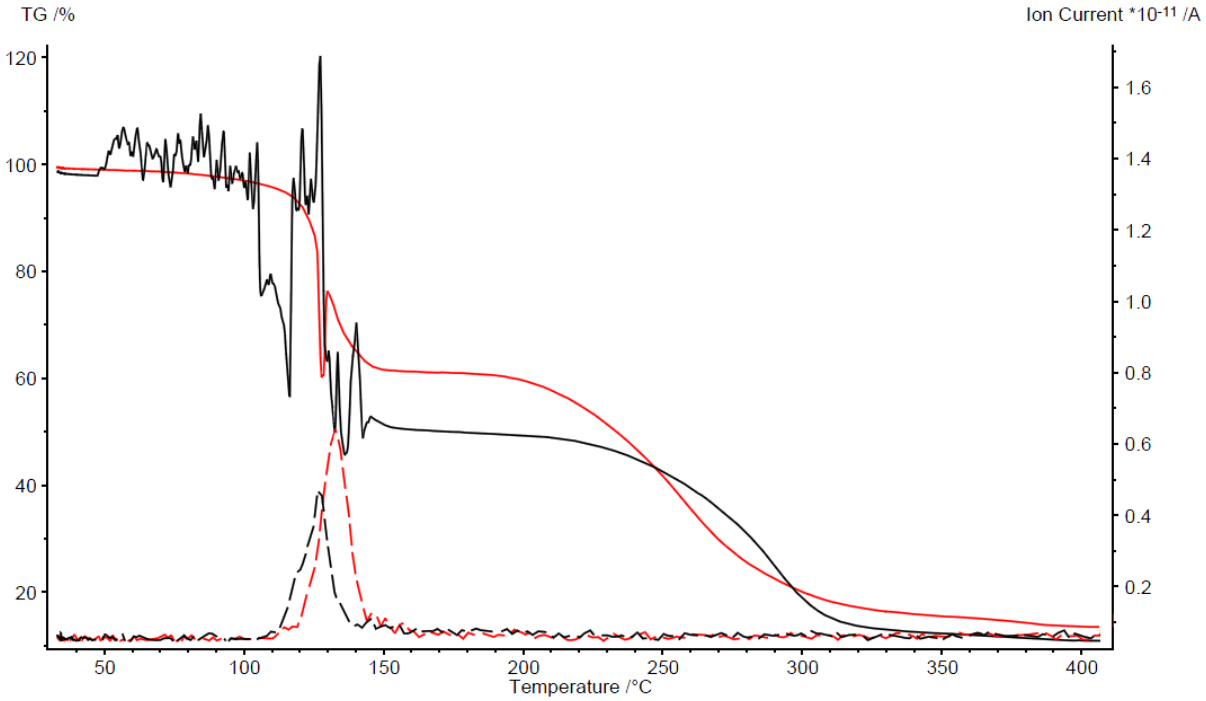

Figure 47: TGA and MS measurements of batteries 1 (black) and 2 (red).